People's Democratic Republic of Algeria
Ministry of Higher Education and Scientific Research
Abderrahmane Mira University of BEJAIA

جامعة بجاية
Tasdawit n Bgayet
Université de Béjaïa

Faculty of Technology
Electrical Engineering Departement
Laboratory of Industrial Technology and Information

PhD Thesis

In Partial Fulfillment of the Requirement for the Degree of

DOCTORATE

Domain: Sciences and Technologies Field: Automatic

Option: Automatic control and Industrial Computing

Presented by
Lylia LARBI

Title

Design of a battery charger circuit with intelligent maximum photovoltaic power tracking control

Defended on December 14, 2025 in front of the Jury composed of:

First last names	Grade		
Mr Said AISSOU	MCA	Univ of Bejaia	President
Mr Abdelhakim BELKAID	Professeur	Univ of Bejaia	Thesis director
Mr Slimane HADJI	MCB	Univ of Bejaia	Thesis co-director
Ms Samia BOURDIM	MCA	Univ of Constantine 1	Examiner
Ms Hadjer BOUNECHBA	MCA	Univ of Constantine 1	Examiner
Mr Hocine LEHOUCHE	MCA	Univ of Bejaia	Examiner

Academic year: 2025/2026

Acknowledgement

First and foremost, my sincere thanks go to my director of thesis **Prof Abdelhakim BELKAID** for the continuous support of my Ph.D. study and related research, for his motivation, and for the time he devoted to the completion of the thesis. Also, I would like to voice my deep thanks to **Dr Slimane HADJI**, whose invaluable advices and support helped greatly in my doctoral trainig.

I sincerely thank **Mr Said AISSOU** from university of Bejaia for honoring me by chairing the thesis jury, and all other members **Mr Hocine LEHOUCHE** from university of Bejaia and **Ms Samia BOURDIM and Hadjer BOUNECHBA** from the university of Constantine 1, for accepting to review this dissertation.

I would also thank all the members of LTII, (Laboratoire de Technologie Industrielle et de l' Information), who have been a true source of inspiration. I would like to thank the entire ESTACA'LAB team at the university of Paris Saclay, where I had the opportunity to complete a short research internship. I particularly thank **Toufik AZIB** for his welcome and kindness, it was an enriching experience.

My family has been my driving force in pursuing doctoral studies. I am deeply thankful specially my husband and my parents, my sister and my brother for their unconditional support and encouragement. I dedicate this work to all my family.

I would thank all my friends, for the friendly atmosphere we have shared over the few past years, and the good times spent together, meals, walks and conversations. A special thanks to Nassima, Cylia, Wazna, and my teachers Ms Taalit BELHOUL,and Ms Sofia BELAID

Table of content

List of figures

List of tables

Acronyms and Symbols

List of acronyms

Photovoltaic Systems

Abbreviation	Description
PV	Photovoltaic
STC	Standard Test Conditions
MPP	Maximum Power Point
MPPT	Maximum Power Point Tracking
P&O	Perturb and observe
IncCond	Incremental Conductance
Isc	Short-Circuit Current
Voc	Open-Circuit Voltage
Vmp	Voltage at Maximum Power
Imp	Current at Maximum Power
CUF	Capacity Utilization Factor
PR	Performance Ratio

Battery Systems

Abbreviation	Description
BAT	Battery
SOC	State Of Charge
DOD	Depth Of Discharge
UPS	Uninterruptible Power Supply

Control Theory

Abbreviation	Description
ANN	Artificial Neural Network
MLP	Multilayer Perceptron
PI	Proportional Integral
PID	Proportional Integral Derivative
ZN-PI	Ziegler-Nichols Proportional Integral
ZN-PID	Ziegler-Nichols Proportional Integral Derivative
OS	Overshoot
RT	Rise Time
ST	Settling Time
IAE	Integral of the Absolute Error
ISE	Integral of the Squared Error

Power Electronics

Abbreviation	Description
DC	Direct Current
AC	Alternating Current
PWM	Pulse Width Modulation
CCM	Continuous Conduction Mode
DCM	Discontinuous Conduction Mode
MOSFET	Metal-Oxide-Semiconductor Field-Effect Transistor
IGBT	Insulated-Gate Bipolar Transistor
BJT	Bipolar Junction Transistor
SEPIC	Single Ended Primary Inductor Converter

Measurement and Interface

Abbreviation	Description
ADC	Analog-to-Digital Converter
GUI	Graphical User Interface

Machine Learning

Abbreviation	Description
MSE	Mean Squared Error
ReLU	Rectified Linear Unit

List of symbols

Symbols used in Chapter 2

Abbreviation	Description
R_s	Series resistance
R_{sh}	Shunt resistance
I_{ph}	Photogenerated current
I_0	Diode saturation current
N_s	Number of series modules
N_p	Number of parallel modules
V_{BAT}	Battery terminal voltage
E_{BAT}	Battery internal voltage
Q_{BAT}	Battery capacity

Symbols used in Chapter 3

Abbreviation	Description
$\mathbf{P_{mpp}}$	Maximum power point power
$\mathbf{V_{mpp}}$	Maximum power point voltage
D	Duty cycle
$\mathbf{K_p}$	Proportional gain
$\mathbf{K_i}$	Integral gain
$\mathbf{K_d}$	Derivative gain
$\mathbf{T_i}$	Integral time constant
$\mathbf{T_d}$	Derivative time constant

List of publications

Article

1. **L. LARBI, A. BELKAID, S. HADJI, N. OUALI, T. AZIB** "Intelligent management of battery charging and discharging for photovoltaic systems *CIGRE Science & Engineering*, affects October 2025 :1-24. "https://cse.cigre.org/cse-n038/intelligent-management-of-battery-charging-and-discharging-for-photovoltaic-systems.html.

2. **Lylia LARBI, Abdelhakim BELKAID, Slimane HADJI, Ilhami COLAK, Said AISSOU, Korhan KAYISLI, Toufik AZIB**. Optimization and control of battery charging/discharging with PV system. *INTERNATIONAL JOURNAL of RENEWABLE ENERGY RESEARCH, August*, 2024. **Under Publication.**

International conferences :

1. **L. LARBI,** A. BELKAID, S. HADJI, "Design of a buck converter battery charging controller in PV plant" ICSMARTGRID 2022 10th International Conference on Smart Grid June 27-29, 2022, Istanbul/Turkey A Hybrid (Real and Virtual) Conference.

2. **Lylia LARBI**, Abdelhakim BELKAID, Slimane HADJI, Ilhami COLAK, Korhan KAYASLI, Nassima OUALI, Said AISSOU. Intelligent battery control for solar systems. 14th International *Conference on Renewable EnergyResearch and Applications ICRERA* 2025, October 27-30, Vienne, Austria.

3. Nassima Ouali, Hocine Lehouche, Abdelhakim Belkaid, Ilhami Colak, **Lylia Larbi,** Abdelyazid Achour, korhan Kayisli, Optimization of Photovoltaic System Using A Predictive Adaptive Rst-Based Controller, 14th International Conference on Renewable Energy Research and Applications (ICRERA 2025), Vienna/Austria, Oct 27-30, 2025,

4. S. Hadji, A. Belkaid, K. Kayisli, I. Colak, S. Aissou and **L. Larbi**, "A Comparative Analysis of Cuk, SEPIC, and Zeta Converters as Maximum Power Point Trackers," *2024 12th International Conference on Smart Grid (icSmartGrid)*, Setubal, Portugal, 2024, pp. 539-544, doi: 10.1109/icSmartGrid61824.2024.10578258.

5. S. Hadji, A. Belkaid**, L. Larbi**, I. Colak, K. Kayisli and S. Aissou, "High Gain Voltage SEPIC Converter for PV System," *2024 12th International Conference on Smart Grid (icSmartGrid)*, Setubal, Portugal, 2024, pp. 618-622, doi: 10.1109/icSmartGrid61824.2024.10578071.

6. S. Hadji, **L. Larbi**, A. Belkaid, I. Colak and R. Bayindir, "Global optimum operating point tracker of PV system, under partial shading, using parallel searching," *2022 10th International Conference on Smart Grid (icSmartGrid)*, 2022, pp. 227-230, Istanbul/Turkey, 27-29 June 2022, doi: 10.1109/icSmartGrid55722.2022.9848552.

National conferences :

1. **L. Larbi**, A. Belkaid, S. Hadji, " Design of a Control strategy for Photovoltaic Generator," *National Conference on Intelligent Energy Management and control of Renewable Energy Systems (NCIEMCRES'24)*, University of Bejaia, Bejaia, Algeria, October 30-31, 2024.

2. **L. Larbi**, A. Belkaid, S. Hadji, N. OUALI " Optimizing Battery Charge Cycles in Solar Energy Systems," *National Conference on Intelligent Energy Management and control of Renewable Energy Systems (NCIEMCRES'25)*, University of Bejaia, Bejaia, Algeria, November 19-20, 2025.

General Introduction

The global energy landscape is undergoing a pivotal transformation, driven by the urgent imperative to mitigate climate change and ensure sustainable development. This transition, underscored by the International Renewable Energy Agency (IRENA) as both an environmental necessity and a profound economic opportunity, is catalyzed by the rapid deployment of renewable energy sources [1]. Among these, solar photovoltaic (PV) technology has emerged as a preeminent force, experiencing exponential growth driven by precipitous cost declines and continuous efficiency gains. Projections, including those from major energy outlooks, confirm solar PV's central role in future energy systems, with its modularity and abundance positioning it as a cornerstone of decarbonization efforts [2].

However, the intrinsic variability of solar irradiance due to diurnal cycles, seasonal shifts, and weather patterns poses a fundamental challenge to its seamless integration. This intermittency creates a critical mismatch between energy supply and demand, complicating grid management and limiting the reliability of standalone systems. Consequently, the coupling of PV generation with energy storage, particularly electrochemical batteries, has become essential to buffer supply, shift energy delivery to times of demand, and ensure power quality and security [3]. This integration is not only relevant to stationary power but is also a critical enabler for the electrification of other sectors, from transportation including pioneering applications in electric vehicles and aviation to maritime propulsion, where hybrid systems are gaining traction [4, 5, 6].

While the concept of PV-battery systems is well-established, optimizing their performance, efficiency, and economic viability remains a significant research challenge. The core complexity lies in the need for sophisticated control strategies that can intelligently manage the non-linear and time-varying interactions between the PV array, the battery, and the load. An effective control system must simultaneously maximize energy harvest from the PV source through precise maximum power point tracking (MPPT), optimize battery cycling to extend its lifespan, and maintain system stability under fluctuating environmental conditions. Advances in areas like wireless charging for electric vehicles highlight the ongoing innovation in system integration and management, pointing toward increasingly intelligent and adaptive solutions [7].

This thesis addresses the control challenge at the heart of efficient PV-battery system operation. It focuses on the development and validation of advanced energy management strategies for standalone systems, with the primary objective of enhancing overall performance through the integration of Artificial Intelligence (AI). The central research aim is to design, simulate, and analyse a novel control system that leverages Artificial Neural Networks (ANNs) to improve upon conventional MPPT and battery management techniques, thereby achieving superior energy capture and storage utilisation under dynamic operating conditions.

The thesis is structured to logically progress from foundational principles to the proposed innovative solution. Chapter 1 establishes the technological context, reviewing PV and battery characteristics and conducting a comparative analysis of system architectures. It justifies the selection of a DC-coupled parallel configuration as the optimal framework for this study, balancing efficiency, flexibility, and control potential.

Chapter 2 delves into the systematic modelling of system components employing the single-diode model for PV panels and an equivalent circuit model for lead-acid batteries and outlines the methodology for system sizing and power converter design.

Finally, Chapter 3 presents the core contribution: the design and implementation of an intelligent management system. This system integrates an ANN-based MPPT algorithm with PI/PID controllers for regulation. Through comprehensive simulation studies, this chapter demonstrates the superior performance of the proposed AI enhanced strategy in optimising power extraction and battery operations compared to conventional methods, validating its potential for more efficient and resilient standalone solar energy systems.

Chapter 1

Technologies and System Architectures for PV-Battery Applications

Table of Contents

1.1. Introduction

The transition to a decarbonized energy system, propelled by the rapid deployment of solar photovoltaic (PV) technology, presents a critical operational challenge: the inherent intermittency and non-dispatchability of solar power. While PV generation, having evolved from silicon to emerging perovskite technologies, offers a clean and increasingly cost-competitive energy source [1, 9], its direct integration into electrical systems can lead to voltage instability, power quality issues, and significant energy curtailment [10, 11]. This variability fundamentally limits the reliability and value of standalone PV systems and complicates large-scale grid integration, underscoring the economic and technical rationale for more resilient distributed generation approaches [8, 13].

To transform solar energy from a variable resource into a reliable and dispatchable one, coupling PV arrays with energy storage, particularly battery (BAT) systems, has become essential. PV-battery hybrid systems mitigate intermittency by storing surplus energy for later use, smoothing power output, and providing critical backup capabilities [13]. However, the mere combination of components is insufficient to guarantee optimal performance, economic viability, or longevity. The overall efficacy of a PV-battery system is profoundly influenced by fundamental architectural decisions, particularly the choice between alternating current (AC) and direct current (DC) coupling for the microgrid. This choice involves critical trade-offs in efficiency, complexity, control, and cost that must be evaluated against application-specific requirements [12, 14].

Current research and industrial implementations reveal a knowledge gap in providing a holistic, comparative framework for these design choices tailored to specific application constraints. While individual technologies are well-understood, the systematic analysis of their integration focusing on the synergies and trade-offs between architecture, power electronics, and control readiness requires further elaboration [14]. This chapter addresses this gap by conducting a comprehensive review and analysis to establish the technological foundation for this thesis.

Therefore, this chapter aims to move beyond a simple catalog of technologies. It positions the architectural design as a primary response to the core problem of PV intermittency and system optimization. We systematically analyze the available solutions to justify the specific technical choices that underpin the subsequent development of advanced control strategies in

this research. The objective is to guide qualitative decisions on system configuration, ensuring the adopted architecture is inherently capable of supporting the intelligent, high-performance management to be developed in later chapters.

This chapter is structured as follows. Section 1.2 provides a foundational overview of the core components: PV generators and battery storage systems, discussing their characteristics, models, and current technological limits. Section 1.3 presents and compares the principal system architectures and microgrid types (AC, DC, hybrid), analyzing their feasibility, applications, and suitability for effective PV-battery integration. Section 1.4 delves into the critical role of power electronic converters, detailing topological options for PV and battery interfacing and describing the resulting energy flow paths and system operational modes. Finally, Section 1.5 synthesizes the analysis to explicitly justify the architectural and topological selections made for this thesis, providing a clear and motivated foundation for the system design detailed in Chapter 2 and 3.

1.2. PV-BAT system

1.2.1. Photovoltaic generator

Many innovations in photovoltaic (PV) cells are currently being developed and are available on the market, including crystalline silicon, thin-film, organic, single-junction and multi-junction technologies. The National Renewable Energy Laboratory (NREL) has collected data on the efficiencies of the main PV cell technologies tested under standard test conditions (STC) since 1976 [15]. In the literature, the majority of authors do not specify the type of PV technology they are modelling. Of those that do, crystalline silicon PV cell technology is generally favoured. Several studies have been carried out on the different PV technologies and their respective advantages and disadvantages [16,17]. Different applications, such as PV houses, pumped irrigation and desalination systems, are analysed in relation to the various PV technologies [18].

For system design, the choice of PV technology has direct implications for the control strategy and sizing of other components. For instance, high-efficiency technologies like heterojunction (HJT) or tandem perovskites can reduce the required area for a given power output, but may present different degradation profiles or initial costs, influencing the cost-benefit analysis of the associated storage [9]. However, accurate modelling of the I-V curve,

essential for Maximum Power Point Tracking (MPPT), remains largely based on the single-diode model, valid for most silicon-based technologies dominant in the market [16].

An array of combined PV cells forms a PV module, while a group of assembled PV modules forms a PV array to supply specified loads. A PV system consists of a PV generator and the system balancing elements (such as power converters, controllers, cabling, protection devices, etc.) that connect the PV generator to AC or DC loads. (Fig. 1.1).

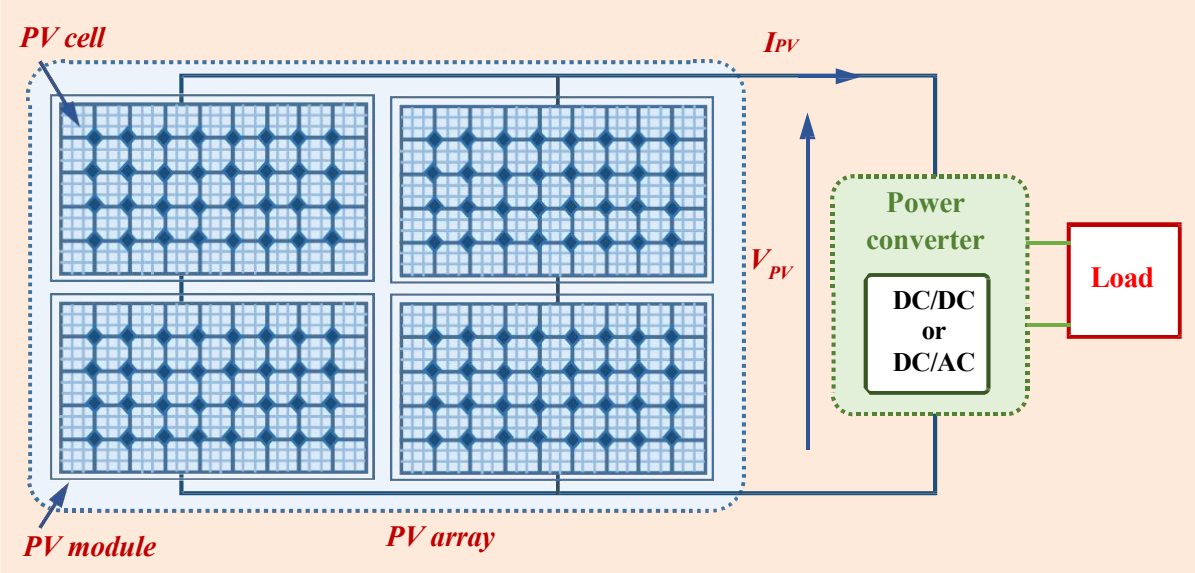

Figure 1. 1. Typical PV system feeding a load (AC or DC).

The principal characteristics of a PV panel are as follows:

- Short circuit current (I_{SC}) is the maximum obtainable current from a PV panel (voltage is zero).
- Open circuit voltage (V_{OC}) is the maximum obtainable voltage from a PV panel (current is zero).
- Maximum power point (MPP) is the maximum power generated by the PV panel at given solar irradiations and temperatures. In fact, when the solar irradiation is decreasing, the current output decreases, and when the temperature is deviating from 25 °C (standard temperature), the voltage decreases, thus in both case the power output decreases.

- Installable capacity, given in "watt-peak" (Wp), referred to the nominal power generated by a PV panel during STC. The STC utilized to test PV panels are: vertical irradiation of 1000 W/m², average panel temperature of 25°C, air mass of 1.5 [19].

- Capacity Utilization Factor (CUF) usually calculable on a yearly cycle, is the ratio between the actual and the theoretical output of the PV system running each hour of the year (8766 hours) over its installed capacity. A show case in India indicates a CUF of PV systems of around 22% [20].

- Performance Ratio (PR) represents the ratio of the actual power output of the PV system to the estimated maximum power output (on the basis of the PV system characteristics, irradiation and temperature profiles...). PR is used to evaluate the performance of the whole PV system, losses in the power converters, cabling ohmic losses, dirtiness on PV panels, etc. In [19] properly conceived PV systems are expected to attain a PR of 80% to 90% during the year. However, the literature review in [21] found that the actual PR is lower (ranging from 55% to 76% for about one hundred PV systems installed in Europe) which emphasizes that the operating conditions of PV systems can be optimized [22, 23].

In order to enhance the dispatchability of PV source and improve the autonomy of the system, an energy storage system can be added [24]. This is the point of the next paragraph.

1.2.2. **Battery system**

BAT storage is widely regarded as a successful strategy for mitigating (and ultimately eliminating) power demand and intermittent PV source power imbalances [25,26]. Many PV sector companies have started creating and marketing storage systems based on BAT technology in response to the need for more reliable energy supply [27]. Some suggestions of when the advantages of combining a PV source with BAT outweigh the additional cost are provided by the scholarly literature [28].

With the exception of references [29, 30], and [31], all writers focus on lead-acid BATs as the most recent low-cost technology for use with PV systems [32] out of the several possibilities for BAT storage that are now available for a summary, see [33, 34, 35]. For our thesis, we have selected lead-acid BAT as the recommended technology, as is the case with the

majority of previous research. However, this choice requires critical justification based on a comparative analysis of technologies. Table 1.1 presents a synthesis of the main trade-offs between lead-acid and lithium-ion batteries, the two most relevant technologies for stationary PV coupled storage.

Table 1. 1. Critical Comparison of Battery Technologies for Stationary PV Applications.

Criterion	Lead-Acid Battery	Lithium-Ion Battery	Implication for System Design
Investment Cost(€/KWh)	Low (50-150)	High (150-400)	Lead-acid favors short term profitability and budget constrained applications.
Energy Density (Wh/kg)	Very Low (30-50)	High (100-265)	Minor impact for fixed stationary storage. Critical for mobility.
Cycle Life (cycle at 80% DOD)	Low (500-1200)	High (2000-7000)	The shorter lifespan of lead-acid increases lifecycle cost, requiring a control strategy to optimize cycles (depth of discharge, current).
Round-Trip cycle Efficiency	Medium (80-85%)	High (95-98%)	Higher losses in lead-acid reduce overall system efficiency and increase PV array sizing requirements.
Self-discharge	Low(1-3%/Month)	Very Low (1-2%)	Negligible for daily cycling.

Technology Maturity & Recycling	Very mature,>99% recycling loop	Maturing, recycling in development	The maturity of lead-acid offers reliability and an established circular economy model.
BMS Requirements	Simple (Voltage/Temperature control)	Complex (cell balancing, strict voltage/temp. Range control)	Reduces the complexity and cost o the battery management system (BMS).

Our choice is justified for a stationary application where weight and footprint are secondary, and where the upfront cost criterion is paramount. This choice also imposes specific constraints on the control strategy to be developed in Chapter 3: it must imperatively limit the depth of discharge (DOD) and high charge/discharge currents to extend battery life.

Lead-acid BAT has a lower energy and power density and a shorter lifespan than other systems. Nonetheless, it is now the most popular technology in PV system applications because of its increased dependability, decreased self-discharge, and cheaper investment and maintenance costs [36, 37].

Figure 1. 2. Typical lead acid in batteries.

According to a number of writers, lithium-ion BATs with better aging properties and higher energy efficiency will ultimately replace lead-acid [38]. Lithium-ion BATs are now 3.5 times more costly than lead-acid BATs and are still at a relatively early stage of development [39]. Furthermore, lead-acid BAT's poor energy and power density for stationary operations is not as noticeable as it is, for instance, in electric automobiles [40,41]. Based on a comprehensive assessment of the literature, the BAT system's round cycle efficiency and self-discharge by day have been set at 81% and 0.03%, respectively [42,43]. A BAT's primary parameters are:

- ✓ Battery capacity: The storage capacity of the BAT is expressed in Ampere hour or Ah. Often BAT capacities are provided for a specified discharge/charge index or C value. The actual capacity is dependent on operation parameters such as load, temperature, etc.

- ✓ Battery voltage: The terminal voltage under operating conditions is referred to the rated or working voltage. This voltage is defined by the manufacturers. It can be 3V, 6V, 12V, 24V…

- ✓ Depth of discharge (DOD): provides a measurement of energy removed from a BAT in percent of its fully charged state. The BAT' state of charge (BAT'SOC) is the difference between the full capacity and DOD of the BAT in percent. If the DOD is 30% then the SOC is (100 - 30) = 70%.

- ✓ Battery life cycle: represents the number of complete charging – discharging cycles a BAT can complete before the rated capacity decreases to less than 80% of its initial nominal capacity. Once the life cycle is complete, the BAT will operate at a decreased capacity.

- ✓ Charging/Discharging Rate or C-Rating: expressed as C/X, where X is the number of hours for complete Charging/Discharging and C is the BAT capacity. If X = 20 h then C-Rate is C/20 or 0.05C. For C/20 and 80Ah BAT capacity then the Charging/ Discharging current will be 80/20 = 4A.

  Self-discharge: is the losses of the electric capacity of BAT due to its internal electrochemical processing when it is not in use. The self-discharging will increase with increasing of temperatures. It is best to store BATs at lower temperature to minimize self-discharging.

1.3. System architecture for PV-BAT systems

Two types of architectures for PV-BAT systems have been proposed in the literature: the parallel one converter architecture and parallel tow converters architecture [44,45]. These architectures differ in the way the PV generator, BAT system and power converters are connected together [46,47]. In addition, each structure needs to have its own control mechanism, which can be distinguished by the degree of complexity. This section will explain the ways in which the components of the PV- BAT system is interconnected and will outline the control strategy required in each structure [48-49].

1.3.1. In-line Architecture: One converter

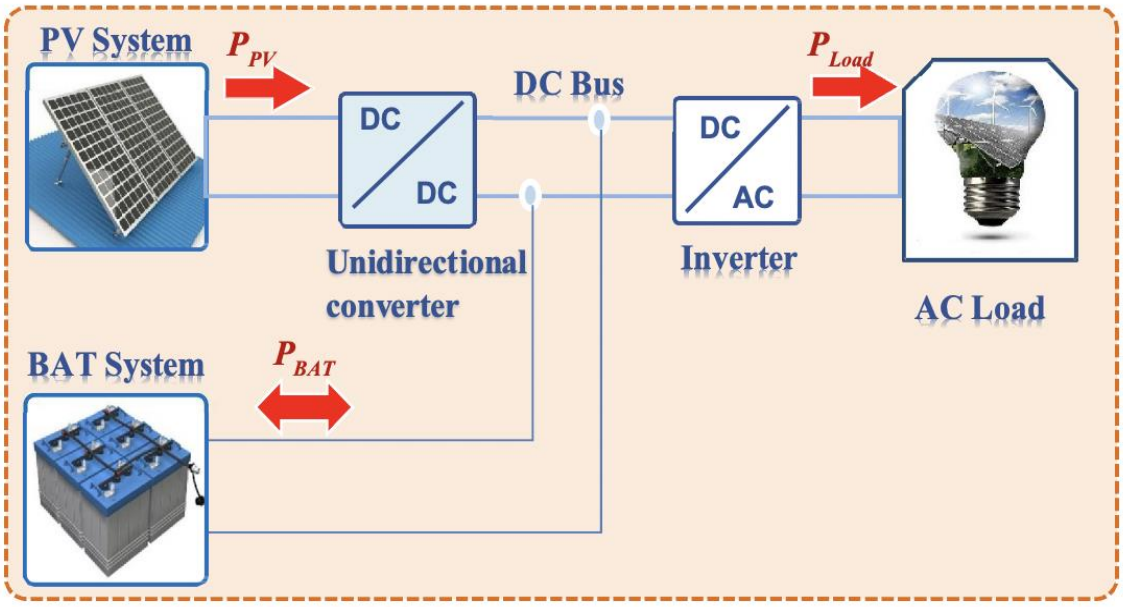

Figure 1. 3. In-line architecture.

In this structure, a DC bus is utilized to connect the PV array and the BAT. A unidirectional DC-DC converter is used as an interconnection between the PV system and the DC bus, whereas the BAT is directly linked to the DC bus. Thus, the voltage of DC bus is fixed by the BAT [50,51]. One application of this structure, for instance, is PV-based uninterruptible power supply (UPS) [52].

In many such cases, the output power of the PV generator is controlled in a way that the BAT'SOC is lower than the maximum. Therefore, the BAT charge current will not exceed its maximum rating. However, the discharging current of the BAT is not controlled [53,54]. Consequently, in these systems, in case of a short circuit on the DC bus it will cause the serious

damages to the BAT. In addition, the BAT numbers have to be such as to attain the requested voltage for the DC bus which limits the flexibility to adapt the BAT and system component sizing and reduces reliability.

Figure 1.3 presents the one converter architecture for the PV-BAT system. The controlling system in this structure consists of the unidirectional DC-DC converter control mechanism with MPPT algorithm.

1.3.2. **DC Coupled Architecture: Two converters**

This structure uses a DC bus as the common link to connect the PV and BAT systems. The PV generator is linked to the DC bus via a unidirectional DC-DC converter, whereas the BAT is also linked to the DC bus using a bi-directional DC- DC converter [55,56].

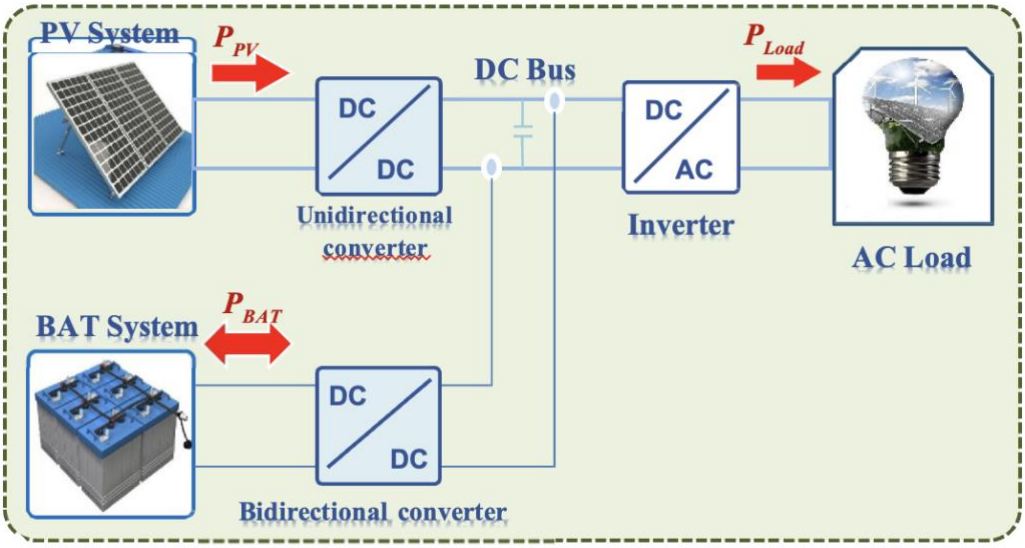

Figure 1. 4. DC coupled architecture.

Through the use of the bidirectional DC-DC converter, the voltage of DC bus can be regulated which allows for more flexibility in choosing of BAT voltage rating and thus improved sizing of the BAT. The BAT discharging current is regulated and at the occurrence of short circuit in the DC bus, BAT is secured. The dimensioning of the inverter is restricted to the combination of PV and BAT power ratings, making this configuration subject to single point failures since the whole power flows via the inverter [57].

The construction of the tow converters for the PV-BAT system is shown in Figure 1.4. The bidirectional DC-DC converter controller and the unidirectional DC-DC converter

controller with MPPT algorithm make up the controlling system in this construction.A critical comparison of these two architectures reveals decisive trade-offs for system performance and safety, as summarized in Table 1.2. This quantitative and qualitative analysis is essential to justify our architectural choice.

Table 1. 2. Comparative Analysis of PV-BAT Architectures.

Evaluation Criterion	In-line Architecture	DC-Coupled architecture	Analysis and Implications
Simplicity & Hardware cost	Advantage: Minimal component count, potentially lower upfront cost	Disadvantage: Additional converter increases complexity and cost.	The lower upfront cost of the *in-line* architecture is attractive but may be offset by higher lifecycle costs (battery replacement).
Overall Energy Efficiency	Medium to High Single conversion stage for PV-Bus Charge. No conversion for battery-Bus discharge	Variable. Two conversion stages to charge battery (PV→Bus→BAT). Battery discharge → bus via converter. Can be optimized by control.	The Two converter architecture can achieve better overall efficiency through independent control optimizing each operating point, despite additional conversion stages.
Control & Flexibility	Limited: Bus voltage imposed	High. Bus voltage independently regulated by bidirectional	architecture enables advanced

	by battery. MPPT possible but battery management is passive (No discharge current control)	converter. Independent and optimal control of MPPT and battery charge/discharge currents.	control strategies (to maximize energy harvest and prolong battery life.
Battery Protection	Critical: battery is directly on the DC bus. A bus short circuit causes massive uncontrolled discharge, irreparably damaging the battery	Robust: Bidirectional converter isolates battery from the bus. Currents are electronically controlled and limited.	Safety and asset protection are paramount requirements. The inability of the *in-line* architecture to protect the battery from faults is a disqualifying disadvantage for a reliable system.
Reliability (single point of failure)	High power path (few components) but failure of the single converter stops the entire system.	The extra converter adds a potential point of failure. However, failure of one converter may allow for degraded modes of operation (e.g., PV-only via inverter bypass if possible).	The Two converter design, while more complex, can be engineered with higher functional redundancy.
Sizing &Scalability	Rigid. Battery nominal voltage determines bus voltage, limiting PV array and battery bank sizing options.	Flexible: PV and battery voltages independent from the bus. Allows optimal sizing of each component and easy system evolution	Essential for adapting the system to variable load profiles or for future upgrades

The in-line architecture offers simplicity and potentially lower hardware cost. However, its inability to control the battery discharge current and, more critically, to protect it from a short-circuit on the DC bus constitutes a major flaw for a system intended for reliable and durable operation [58]. The DC-coupled architecture, although slightly more complex and costly upfront, allows for independent and optimal control of the PV source and storage, robust regulation of the bus voltage, and intrinsic battery protection. Moreover, power balancing might thus be represented by the DC bus voltage, allowing for the study of control system performance and power flow operation in terms of control sophistication. Thus, the parallel two converter's structure system design was chosen for the PV-BAT system in this research.

1.4. PV-BAT power flows

1.4.1. Topologies

DC-DC converter topologies are utilized to fulfill the required load, control the DC voltage, and provide the best possible power transmission. Boost, buck, buck-boost, cuk, flyback-boost, and Single Ended Primary Inductor Converter (SEPIC) are some of the types of DC converters that can act as switch mode controllers, regulating the DC voltage and converting it to the desired operating voltage by increasing or decreasing the output of DC voltage [59-61]. Pulse Width Modulation (PWM) commutation is used to activate the DC-DC converters and regulate their frequency, phase, and amplitude [62,63].

Depending on the needs of the application and the circuit design specifications, power commutating devices for PWM switching, such as MOSFETs, IGBTs, BJTs, and thyristors, are used. A gating control circuit must be used to envision sufficient gating control signals in order to operate the power commutating device [60], [64].

Voltage gain (AV), current gain (Ai), input impedance (Ri), boundary filter inductance (L_b), and minimum filter capacitance (C_{min}) are the parameters that may be used to describe each converter's performance. The continuous conduction mode (CCM) and the discontinuous conduction mode (DCM) are the two different operating modes of the converter. Because of its great efficiency and effective use of passive components and semiconductor switches, the CCM is recommended. Applications with unique control needs may make advantage of the DCM [62]. The minimum inductance value required to ensure that the chopper is operating in the CCM is the inductance value (Lb). The minimum capacitance value needed to lower the ripple

voltage to a predetermined value is known as the capacitance Cmin. The application goal and topology should guide the selection of the appropriate converters.

The two primary converters utilized in PV-BAT systems are the PV DC-DC converter and the BAT DC-DC converter. The power flow of these components should be studied in order to choose the kind of converter. In contrast, the BAT has both energy generating and storage capabilities, whereas PV can only generate energy. Accordingly, bidirectional DC-DC converter topologies are utilized for BAT systems based on the direction of power transfer, whereas unidirectional DC-DC converters are favored in PV systems. PV uses a variety of unidirectional DC-DC converter topologies. According to some earlier research, these converters are generally divided into isolated and non-isolated categories.

The architectures of unidirectional DC-DC converters utilized in PV systems are depicted in Figure 1.5. The boost converter architecture, depicted in Figure1.5(a), is the most often used in the literature because of its many advantages, such as its affordability and ease of use [38], [65]. Nevertheless, there are more output voltage ripples with this architecture [66-68]. To reduce the output voltage ripple in the boost converters, bigger capacitors are needed, which results in a somewhat higher volume [69]. The two-phase interleaved boost converter topology depicted in Figure 1.5 (b) to reduce the voltage ripple [70-71]. In this configuration, the DC bus is connected in parallel to two boost converters with the same ratings. As a result, the input current is distributed across the branches, ensuring good PV power transmission and lowering the current stress on the devices. Additionally, compared to a normal boost converter, the voltage ripples in a 2-phase interleaved boost converter are decreased by a ratio of $\frac{1}{4}$ [72].

A four-leg floating interleaved boost converter, as depicted in Fig. 1. 5 (d) [73] to further reduce the output voltage ripple. In order to reduce the voltage stress on the commutating devices, the output voltage ratio is raised while maintaining the same duty cycle [73].

For the battery bidirectional converter, the non-isolated bidirectional buck-boost topology (Fig. 1.5b) was selected. It is the most prevalent topology for this application due to its structural simplicity, relatively simple control, and good efficiency [81,82]. It allows stepping up (boost mode) or stepping down (buck mode) the battery voltage to match the regulated DC bus voltage, providing the sizing flexibility identified Galvanic isolation, although advantageous for safety, was dismissed for this study to prioritize efficiency and reduce complexity and cost, as the application is a low-voltage system with appropriate safety measures.

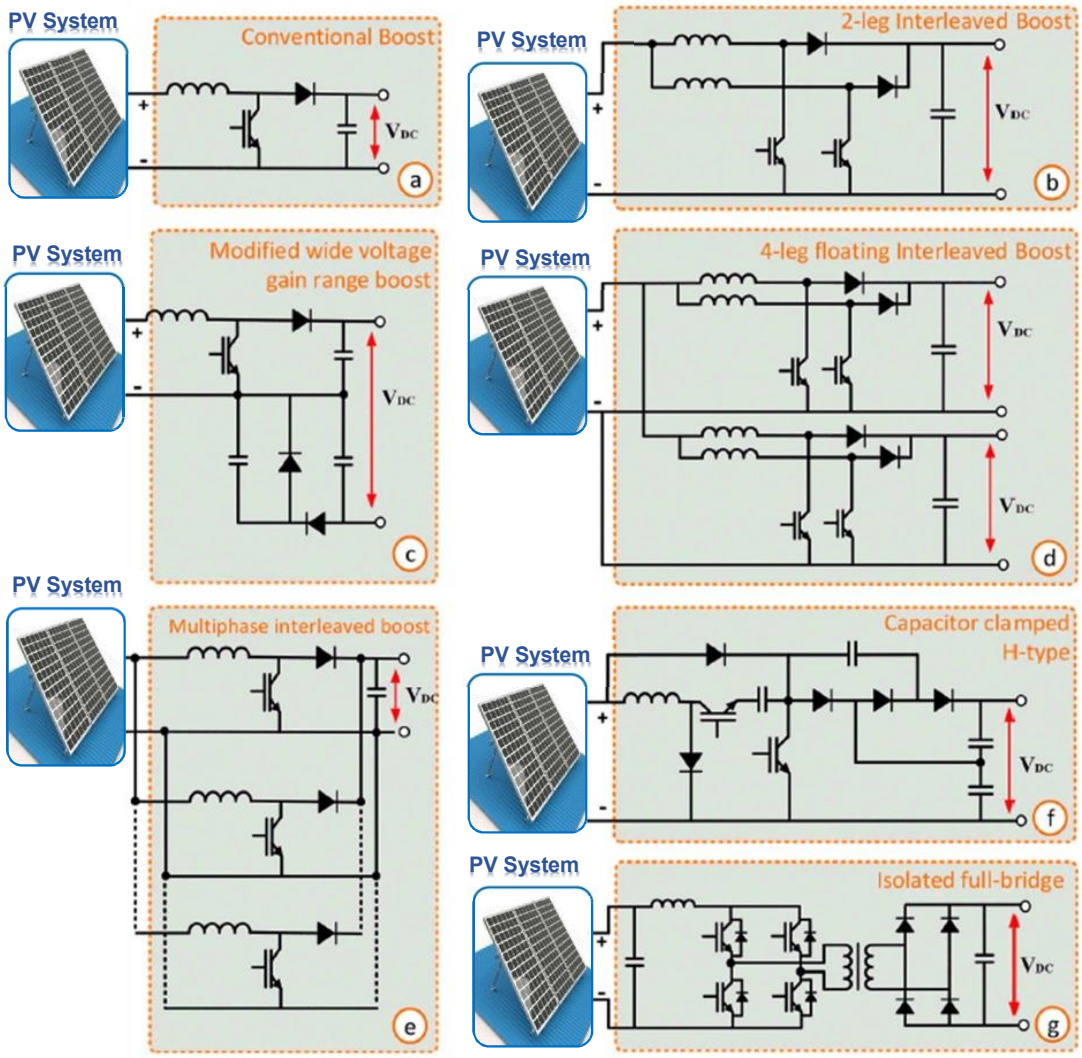

Figure 1. 5. Topologies for unidirectional DC-DC converters in photovoltaic systems.

A multiphase interleaved converter, depicted in Fig. 1. 5(e), in addition to the interleaved boost converters previously mentioned [74].

To enhance voltage gain ranging [75] proposes a distinct boost converter construction called a modified wide voltage range gain boost, which is depicted in Fig. 1.5(c). uses an enhanced voltage gain boost converter to increase the output voltage gain when two boost converters are cascaded [76]. This topology's main advantage is that it just requires one switch component to achieve these significant voltage increases.

As seen in Fig. 1. 5(f) [77], a capacitor clamped H-type boost converter is an additional unidirectional DC-DC converter topology. This design avoids narrow PWM signal pulsing while offering high voltage gain opportunities.

The isolated full-bridge boost converter topology depicted in Fig. 1.5(g) [78]. In this setup, the PV system is separated from the DC bus by a transformer. In this manner, the PV modules may be safeguarded in the event that the DC bus sides failed. Additionally, altering the transformer's transformation ratio could result in a higher voltage gain [79,80]

For PV-BAT hybridization applications, bidirectional DC-DC converter architectures have also been researched whenever an auxiliary storage device is used. The most widely used topology among these is the bidirectional buck-boost converter, which is seen in Fig. 1.6(a) [81,82]. This architecture uses two commutating components and has a straightforward structure and working principle. As for the unidirectional DC-DC converter, by connecting the switches and inductors in parallel, as illustrated in Fig. 1.6(b), the bidirectional buck-boost converter could be converted to the interleaved topology.

A modified SEPIC bidirectional DC-DC converter architecture is used [83], as seen in Fig. 1.6(c). Small voltage strains on the commutating devices and a high input voltage conversion ratio are characteristics of this construction.

In order to increase power, [84] built a modular multiple-input converter, which is another bidirectional DC-DC converter topology, as shown in Fig. 1.6(d). BATs can be shared into two or more inputs and then sent to the DC bus using this structure.

A bidirectional isolated dual full-bridge converter is suggested [78-85] as shown in Fig. 1.6(e). This arrangement is ideal for separating the BAT from the DC bus and lowering the strain on the switching parts.

In conclusion, power flow directions, isolations, the number of switching components, and application complexity are used to categorize the DC-DC converter topologies that are appropriate for PV-BAT hybrid systems. Operating safety, cost, and complexity can all be taken into account when choosing one of these converter topologies.

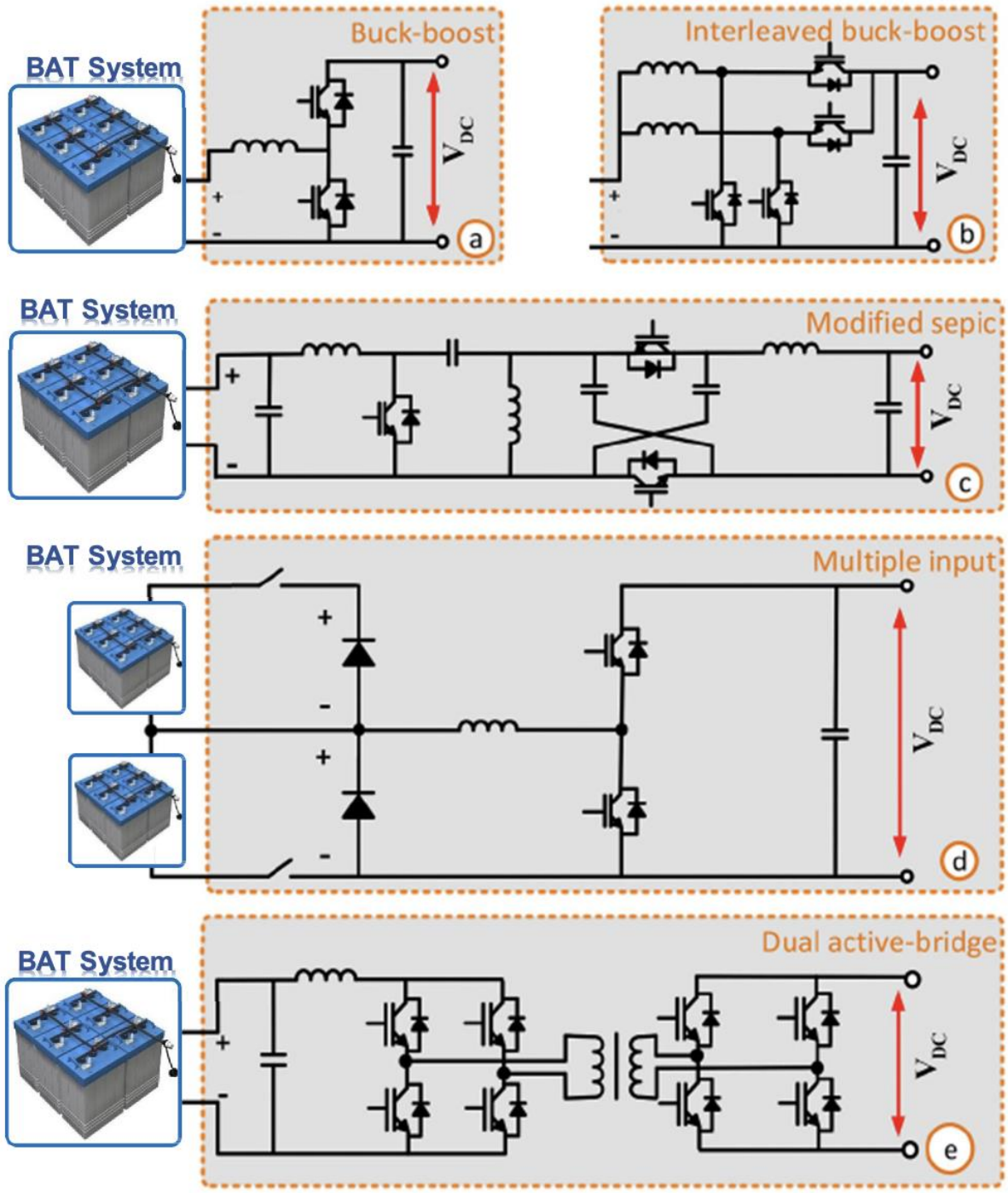

Figure 1. 6. Bidirectional converter topologies for battery systems.

1.4.2. **Operations**

Control strategies for PV-BAT systems remain an active area of research. A literature review was provided to this end. Furthermore, a novel strategy for DC bus voltage regulation and power management has been proposed [86-87].

Potential power flow modes for PV-BAT hybridization applications with two parallel DC-DC converter architectures are depicted in Figure 1.7, and Table 1.1 details how each converter operates in each mode.

Mode 1: PV modules are connected, the inverter is running, the DC-DC buck-boost bidirectional converter is operating on boost, the unidirectional DC-DC boost converter is operating on MPPT, and the BAT is in discharge mode.

Mode 2: The PV generator is connected, the buck-boost bidirectional converter is operating on buck, the inverter is turned on, the load is powered, the boost converter is operating on MPPT, and the BAT is in charge mode.

Mode 3: Entails disconnecting the PV panels, turning off the DC-DC boost converter, turning on the discharge mode of the BAT, turning on the DC-DC buck-boost bidirectional converter, running the inverter, and supplying the load.

Mode 4: The PV array is connected, the inverter is operating, the load is powered, the unidirectional converter is operating on curtailment function, the BAT is operating on discharge, and the bidirectional converter is operating on boost mode.

Mode 5: This mode represents a full system shutdown where all active power processing is halted. The energy sources (PV and batteries) are isolated from the DC bus, the power converters are switched off, and the load is disconnected. This operational state is typically employed in standalone (off-grid) installations or for peak demand reduction strategies.

Mode 6: In this configuration, power is supplied solely by the photovoltaic source. The DC-DC converter operates in Maximum Power Point Tracking (MPPT) mode, while the battery storage is disconnected to prevent any charge/discharge cycling. The inverter is activated and supplies energy coming exclusively from the PV array.

Mode 7: In this mode, the photovoltaic array is connected to the system. The boost converter performs Maximum Power Point Tracking (MPPT) to optimize energy harvest, which is then

directed to charge the battery via the buck-boost converter operating in buck mode. The inverter remains deactivated, and the AC load is consequently disconnected from the system.

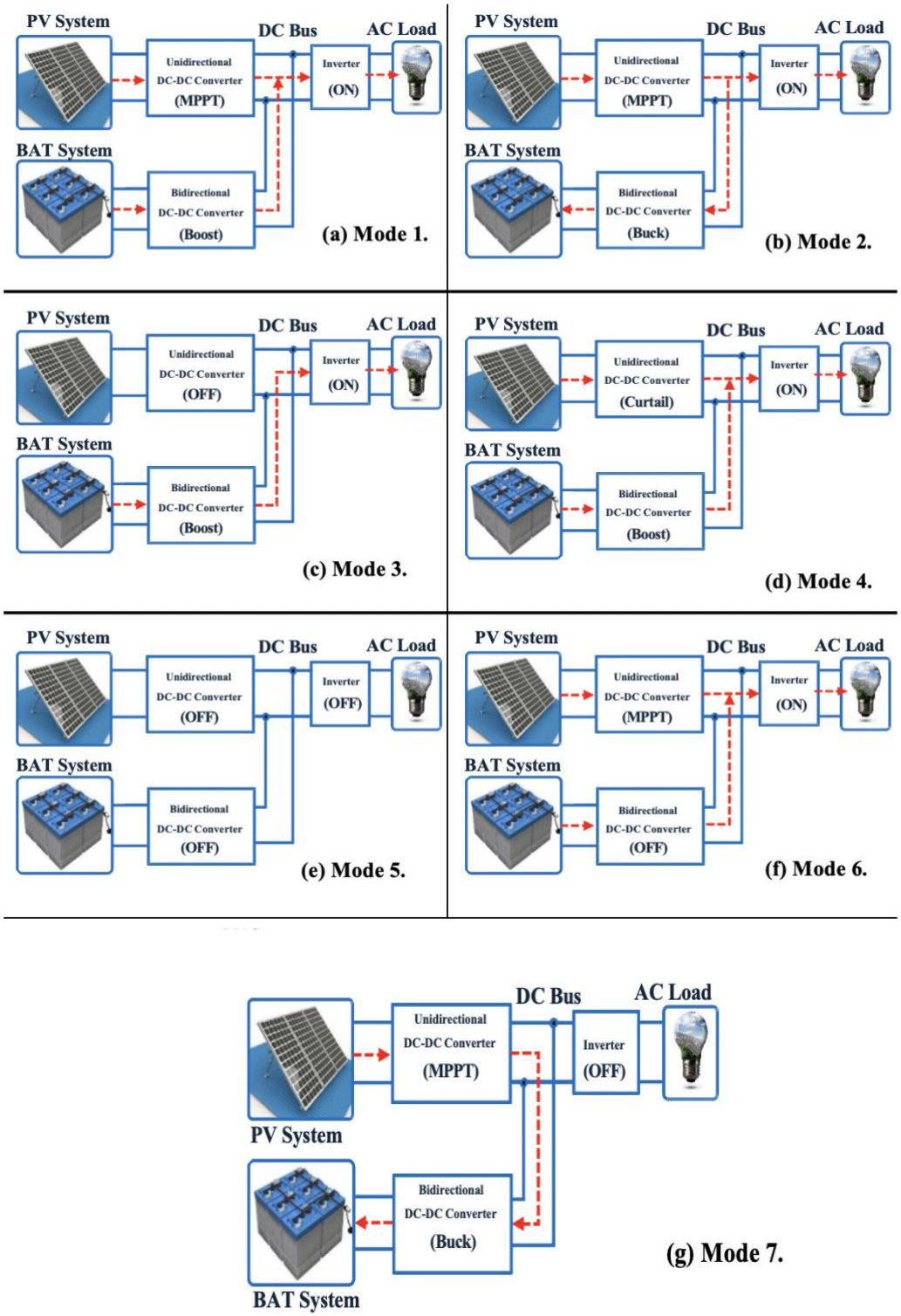

Figure 1. 7. Power flow modes in PV-BAT system.

Table 1. 3. Operational Modes of the PV-BAT System.

Mode	Primary condition	PV converter (Boost)	BAT converter (Buck-Boost)	Inverter	Description of energy flow
Mixed Supply (PV+BAT)	$P_{PV}<P_{Load}$	MPPT	Boost (Discharge)	ON	PV supplies its max. Battery covers the deficit to power the load.
Battery Charge (PV>Load)	$P_{PV}>P_{Load}$	MPPT	Buck (Charge)	ON	PV powers the load and surplus charges the battery
Battery Supply Only	Night/PV unavailable	OFF (Or standby)	Boost (Discharge)	ON	Battery alone powers the load. PV disconnected.
PV Curtailment +Battery Support)	$P_{PVmax} >P_{Load,}$ Low Battery	Current Limiting (curtailment)	Boost (Discharge)	ON	PV is voluntarily limited, battery provides the complement. (SOC management).

System Shutdown	Maintenance/Fault	OFF	OFF	OFF	All sources and loads are isolated
PV Supply Only	$P_{pv}=P_{Load}$, Battery full/disabled	MPPT	OFF	ON	PV directly powers the load. Battery floating or disconnected.
Forced Battery Charge (No AC load)	PV available, AC load zero /disabled	MPPT	Buck (Charge)	OFF	All PV production is directed to battery charging.

1.5. Conclusion

This chapter has presented a comprehensive retrospective analysis of recent PV systems integrated with battery (BAT) storage devices, as documented in the literature. A qualitative comparison of various system architectures was conducted, leading to the selection of a specific PV-BAT configuration. The systems were evaluated based on their architectural design, converter topologies, isolation requirements, and the capability for bidirectional DC power flow.

The chosen architecture for the PV-BAT system is the dual-converter parallel structure. The power electronics for this configuration comprise a unidirectional boost converter for the PV array and a bidirectional buck-boost converter for the battery storage unit.

The methodology employed in this selection phase was therefore structured in two steps. First, an in-depth comparative analysis of existing solutions established a critical evaluation framework, centered on fundamental technical criteria for system performance and integration. Second, based on this analysis, the choice was justifiably made in favor of the parallel dual converter architecture. This configuration offers an optimal compromise, combining the simplicity and efficiency of a dedicated converter for photovoltaic power extraction with the

flexibility and granular storage control provided by the bidirectional battery converter. Thus, the hardware foundation of the system is defined to meet the identified requirements.

However, this state-of-the-art review highlights gaps that the subsequent chapters of this thesis will address:

1. Modelling Needs: Accurate modelling suitable for control of the components (PV and lead-acid battery) is required to design effective strategies.
2. Control Requirements: The system controller must satisfy several often conflicting objectives:

- Decoupling of Dynamics: PV voltage variability must be decoupled from DC bus dynamics to ensure its stability.
- Optimized Battery Management: The bidirectional energy flow with the battery must be controlled to regulate the bus voltage while respecting lead-acid battery constraints (depth of discharge, charge currents).
- Maximum Energy Extraction: The architecture must support a high-performance MPPT algorithm independent of storage control.
- Robustness: The control system must maintain DC bus voltage regulation under variable conditions (partial shading, transitions between battery charge/discharge modes).

Chapter 2

System Modelling and Strategy Control

Table of Contents

2.1. Introduction

Following the architectural analysis in Chapter 1, this chapter details the system modeling, system sizing, and foundational control principles for the selected DC-coupled, dual-converter PV-Battery (PV-BAT) system. The architecture, as shown in Figure 2.1, consists of a photovoltaic (PV) array interfaced via a unidirectional DC-DC converter, a battery (BAT) bank connected via a bidirectional DC-DC converter, and a common DC bus feeding an inverter and load.

Designing an efficient and reliable standalone system requires accurate component models to predict behavior, a rigorous sizing methodology to meet energy autonomy requirements, and robust control strategies to manage power flows[91,92,93]. The inherent nonlinearity and variability of the PV source and the complex electrochemical behavior of the battery necessitate control strategies that are more sophisticated than conventional linear approaches[94,95]. The fidelity of the models developed here directly informs and justifies the need for the advanced control techniques, such as Artificial Neural Network (ANN) based MPPT, which will be presented and validated in Chapter

This chapter is structured as follows: Section 2.2 presents the mathematical models for the PV panel and the lead-acid battery. Section 2.3 outlines the systematic methodology for sizing the PV array and battery bank, supported by a numerical example. Section 2.4 details the design of the power electronic converters. Section 2.5 introduces the core control algorithms, including the Perturb and Observe (P&O) and ANN-based Maximum Power Point Tracking (MPPT) techniques, as well as the Ziegler-Nichols tuned PI/PID controllers for voltage regulation. Finally Section 2.6 describes how these individual models are integrated into a global simulation framework in MATLAB/Simulink.

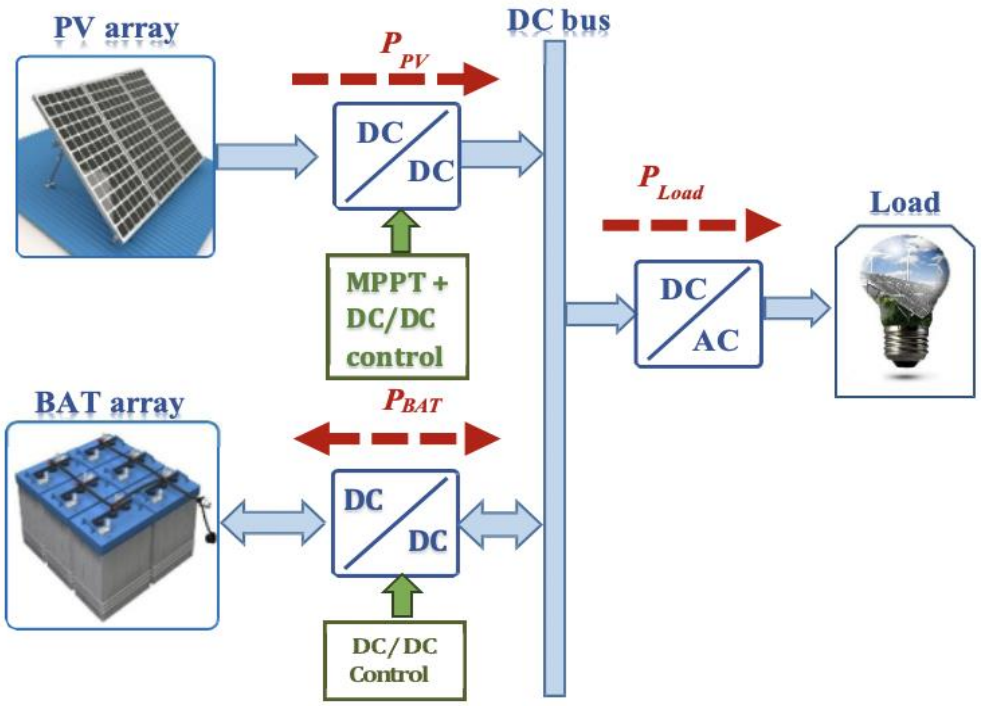

Figure 2. 1. Conventional parallel architecture for photovoltaic-battery systems.

2.2 System modeling

This work does not aim to propose new mathematical models. Instead, it relies on an in depth literature review to identify, evaluate, and select established models best suited to the specific context of this PV-Battery system[94, 99]. A rigorous selection process was conducted to choose appropriate models for the main components[96,97,98], namely the photovoltaic (PV) panels and the battery state of charge (SOC) [100]. The primary criterion was to select models that accurately capture the essential physical behaviors and interactions between components, while maintaining a level of simplicity conducive to system-level simulation and analysis.

The selected models, drawn from the existing body of research, enable a coherent representation of the system dynamics. This approach makes it possible to account for critical interactions such as the impact of solar irradiance on PV output and the nonlinear charge/discharge characteristics of the battery within a manageable computational framework. The overall system, integrating these literature-based component models, will be implemented and simulated using the MATLAB/Simulink software environment to validate the proposed architecture and control strategies.

2.2.1. Model of photovoltaic panel

The energy produced by photovoltaic (PV) panels can be assessed by developing a mathematical model that calculates the electrical energy generated based on solar radiation and ambient air temperature. This analysis focuses on monocrystalline silicon solar panels and employs a single-diode model for the PV cells. Additionally, a series resistor is incorporated to account for internal losses within the cell. The electrical model used in this study is the single-diode equivalent circuit model (see Figure 2.2) [101,102].

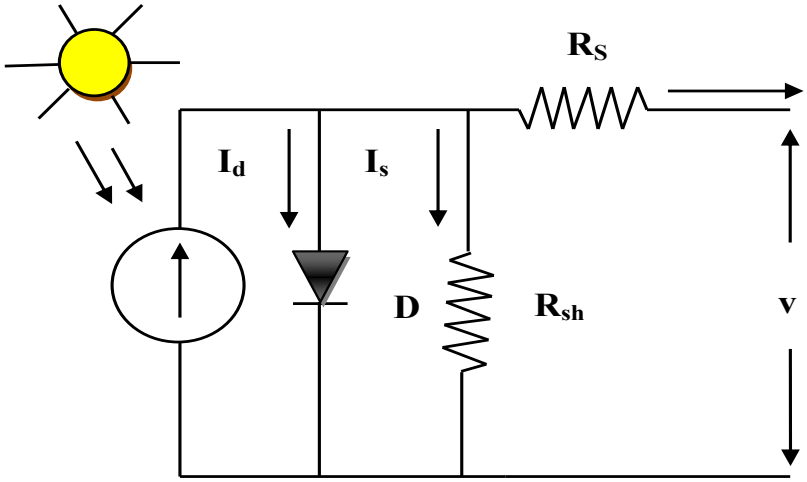

Figure 2.2. Equivalent circuit diagram for the general photovoltaic cell model.

The model accounts for the resistive properties of the cell, represented by a series resistor (R_s), and also considers leakage currents, which are modeled by a parallel resistor (R_{sh}).

$$I = I_{ph} - I_d \left\{ e^{\frac{q(V+R_s I)}{nKT}} - 1 \right\} - \frac{V + R_s I}{R_{sh}} \tag{2.1}$$

In this context, K represents Boltzmann's constant, while T denotes the surface temperature of the photovoltaic cell.

A photovoltaic panel, or module, is created by connecting multiple photovoltaic cells either in series or in parallel. By further connecting several photovoltaic modules together in series and/or in parallel, a photovoltaic array is formed. The model of a photovoltaic panel can be represented as follows:

$$\begin{cases} I_{PVarray} = N_p \times I_{PV} \\ R_{array} = N_s(R_s + R_{sh}) \end{cases} \quad (2.2)$$

In this context, N_s represents the number of modules connected in series, while N_p indicates the number of modules connected in parallel. The P-V (Power-Voltage) and I-V (Current-Voltage) characteristic curves for the first photovoltaic source are provided under standard conditions of 25°C and 1000 W/m² for reference purposes. Additionally, the I-V and P-V characteristic curves at various solar irradiance levels and temperatures are illustrated in Figure 2.3.

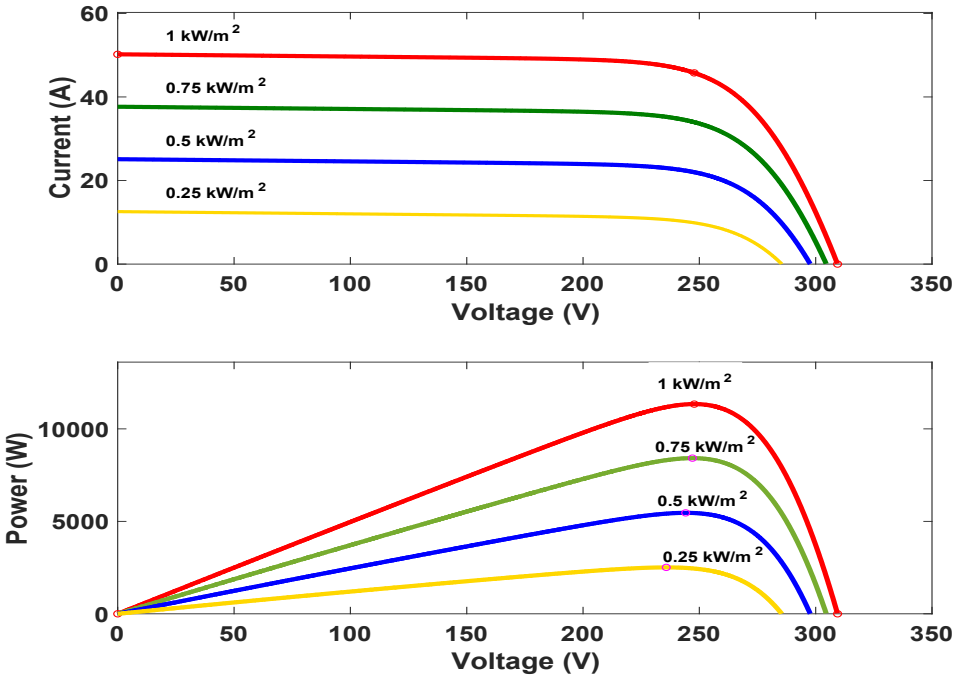

Figure 2. 3. I-V and P-V curves for varying input parameters.

The (I-V) and (P-V) characteristics indicate that the power produced by a PV panel is directly proportional to irradiance and inversely proportional to temperature.

Equation (2.3) [103] quantitatively demonstrates how temperature and solar irradiance affect the photogenerated current (I_L).

$$I_{pv} = (I_{pvn} + K_i \Delta T)\frac{G}{G_n} \quad (2.3)$$

This relationship arises because the series resistance (R_s) in photovoltaic cells is significantly lower than the shunt resistance (R_{sh}), allowing the approximation that the short-circuit current (I_{sc}) equals the minimum photovoltaic current. The system employs the following notation:

- I_{pvn}: Nominal photovoltaic current
- K_i: Current temperature coefficient
- ΔT: Deviation from nominal temperature
- G: Actual solar irradiance
- G_n: Standard test condition irradiance

The array configuration consists of two parallel branches, each containing four series-connected panels. Individual panels are rated at 135 W with these key characteristics:

- Maximum Power Point: 243 V / 50 A
- Open-Circuit Voltage: 22 V
- Short-Circuit Current: 8.36 A

This 8 panels array delivers a cumulative output of 12000 W. As depicted in Figure 2.3, variations in solar irradiance dynamically alter the system's current-voltage (I-V) and power-voltage (P-V) characteristics.

2.2.2. Lead-acid battery model

This study employed a generic lead-acid battery (BAT) model, as described in references [101,103,104]. This type of model is well-established for energy flow analysis in microgrid applications [61,68]. The model calculates two key parameters that represent BAT performance: terminal voltage (V_{BAT}) and state of charge (SOC), illustrated in Figure 2.4.

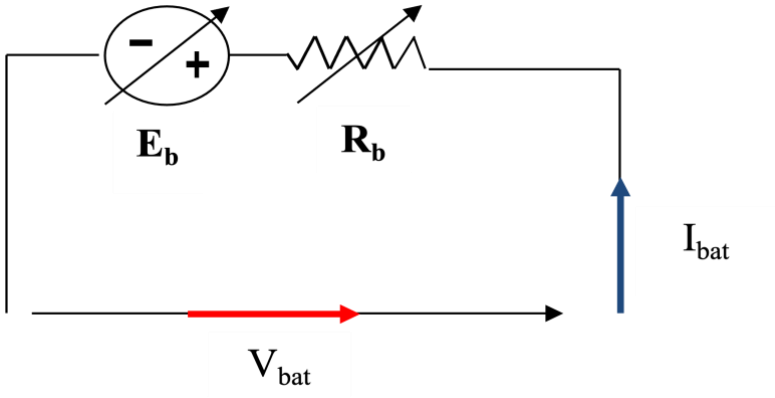

Figure 2. 4. Enhanced standard battery model

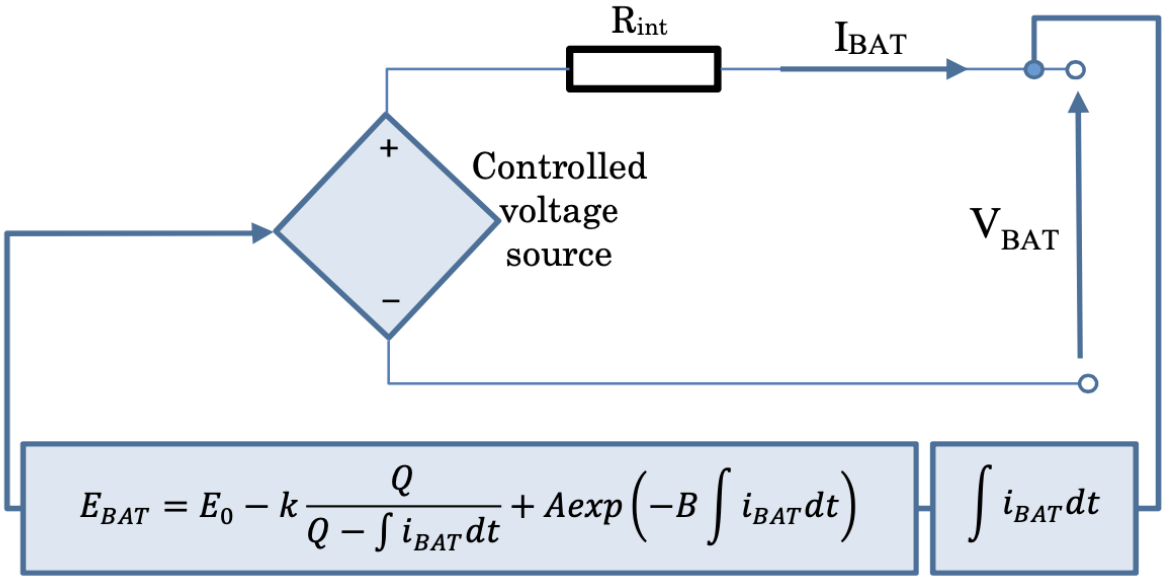

Figure 2. 5. Non-linear standard battery model.

$$V_{BAT} = E_{BAT} - R_{in} \times I_{BAT} \tag{2.4}$$

$$SOC = 100(1 - \frac{\int I_{BAT}\, dt}{Q_{BAT}}) \tag{2.5}$$

$$E_{BAT} = E_0 - k\,\frac{1 - SOC}{SOC} Q_{BAT} + Aexp\{-B(1 - SOC)Q_{BAT}\} \tag{2.6}$$

The model incorporates parameters (Figure 2.5) such as E_0, which characterizes the battery's open circuit voltage, along with Q and R_{int} to represent its capacity (measured in ampere-hours, Ah) and internal resistance (in ohms, Ω), respectively. Additionally, K denotes the polarization constant (in volts per ampere-hour, V/Ah), A signifies the exponential voltage

amplitude (in volts, V), and B quantifies the exponential capacity coefficient (in inverse ampere-hours, (Ah)−1) [104].

This model focuses on the fundamental electrical dynamics (voltage-SOC-current relationship) critical for real-time energy management and DC bus stability. While temperature compensation and aging effects are crucial for long-term capacity estimation and lifecycle analysis, they are excluded from this core dynamic model for two reasons:

1) The primary control objective is real-time power flow optimization and voltage regulation, which depends more on instantaneous SOC and internal resistance than on slow-varying parameters like capacity fade.

2) This simplification reduces computational complexity, facilitating faster simulations and a more straightforward implementation of the real-time control algorithms. For a complete system assessment, these factors would be integrated into a separate supervisory long-term health management layer.

2.3. System Sizing

The sizing procedure identifies the optimal number of components required to design a cost-effective and high-performing standalone PV-battery (PV-BAT) system [102,105]. The component quantities are calculated to prevent power supply interruptions during periods of high energy demand, while adhering to the system's operational constraints.

The primary objective is to ensure the backup system achieves a high level of autonomy, delivering uninterrupted power supply to the household at a reasonable overall cost. The study incorporates realistic technical constraints, including grid subscription limits, the charger's rated current, the maximum allowable current for battery injection, and the DC bus voltage. A critical consideration is the configuration of photovoltaic (PV) panels and batteries in series-parallel arrangements to maintain a DC bus voltage that is a multiple of 6 V, introducing additional sizing complexities.

Energy flow is meticulously forecasted, as precise system sizing demands rigorous coordination between all components of the installation such as the PV array, battery bank (BAT), and load requirements. This coordination ensures optimal performance, balancing energy generation, storage, and consumption efficiently.

2.3.1. Electricity Demand Assessment

The electricity demand assessment involves calculating the daily electrical energy consumed by end-users [106,107], expressed in watt-hours per day (Wh/day) or kilowatt-hours per day (kWh/day). The methodology, adapted from [108], involves the following steps:

- **Inventory of Electrical Devices**: Identify all appliances powered by the standalone photovoltaic (PV) system and document their rated operating power (in watts).
- **Usage Duration Estimation**: Determine the daily operating hours for each device.
- **Energy Consumption Calculation**: Multiply the rated power (W) by the daily usage duration (hours) to compute the daily energy consumption (Wh) per appliance.
- **Aggregate Demand**: Sum the individual energy values to derive the total daily electricity demand.
- **Performance Ratio (PR)**: The performance ratio quantifies inherent losses within the electrical installation. Represented as a dimensionless value between 0 and 1 (or 0% to 100%) [109], it serves as a critical metric for evaluating system efficiency [109,110].

This inventory provides a comprehensive overview of system power and energy requirements. Electricity demands and daily energy consumption were quantified in the prior inventory, enabling the establishment of a detailed power and energy balance.

2.3.2 PV Array Sizing

Based on the evaluated electrical load and solar potential, the PV array configuration is determined. The first step involves computing the total number of modules required for the installation using Equation (2.7) [111]:

$$N_{PV} = \frac{P_c}{P_r} \tag{2.7}$$

where:

- N_{PV} represents the total number of PV modules;
- P_c corresponds to the peak power output of the photovoltaic array;
- P_r denotes the rated power of a single PV module.

A straightforward analytical formula can be applied to determine the peak power capacity of the PV array (P_c) in equation (2.8) :

$$P_c = \frac{E_c}{E_i} \times \frac{P_i}{R_p} \tag{2.8}$$

The photovoltaic (PV) system's key parameters are defined as follows:

- P_c represents the peak power output of the PV array, corresponding to its maximum achievable power under ideal operating conditions.
- E_c quantifies the daily electrical energy output (in kWh/day) potentially generated by the system.
- P_i denotes the irradiance level under standard test conditions (STC), measured in kW/m².
- E_i reflects the total daily solar irradiation (in kWh/m²/day) incident on the PV array.
- R_p characterizes the system's performance ratio, a dimensionless metric that evaluates overall efficiency by accounting for energy losses.

2.3.3 Battery Sizing Methodology

The battery capacity must be sufficient to meet all electrical demand (E_c). When sizing the battery bank, the following design criteria are applied [89, 90] to ensure reliability and cost-effectiveness [102,105]:

- **Reserve autonomy period (NJ)**: Ensure continuous power supply during periods of zero solar energy contribution.
- **No solar input**: Account for scenarios where photovoltaic generation is unavailable.
- **Depth of discharge limit (PD)**: Maintain operation within the maximum allowable depth of discharge to preserve battery longevity.

Here, PD refers to the maximum permissible depth of discharge for a battery. It is therefore critical to determine the required number of batteries and their series/parallel configuration in accordance with manufacturer specifications.

The total battery capacity (CT) is calculated using the following expression:

$$CT(Ah) = \frac{(Ec \times NJ)}{(PD \times UT)} \tag{2.9}$$

The parameters are defined as follows:

- NJ represents the number of consecutive days with insufficient solar irradiance.
- E_c denotes the daily energy output (in kWh/day) generated by the photovoltaic (PV) system.
- UT corresponds to the nominal operating voltage (e.g., 12 V, 24 V, 48 V) of the battery bank (BAT).
- PD indicates the maximum allowable depth of discharge (DoD) for the batteries, a critical factor for preserving lifespan.

Once the battery capacity is established, the number of parallel-connected battery units (Nb) can be computed.

2.4. Power Converter Design and Optimization

The design of power converters is a cornerstone of modern power electronics, enabling efficient energy management in renewable systems [112,113].

To realize high-efficiency, high-power-density converter topologies, this section details a design methodology incorporating key parameters: switching frequency, magnetic core, copper windings, semiconductor devices, and capacitors. Selection of the switching frequency directly influences passive element size and semiconductor loss mechanisms. Conversely, judicious component selection serves to mitigate these losses.

2.4.1. Power Converter for Photovoltaic Systems

To achieve DC bus compatibility, the PV generator's output is processed by a unidirectional boost converter [109,114]. Through controlled switching actions, this topology steps up the relatively low PV voltage to a utilizable higher DC level, analogous to an inverted buck converter operation [115,116]. The circuit diagram is provided in Figure 2.6.

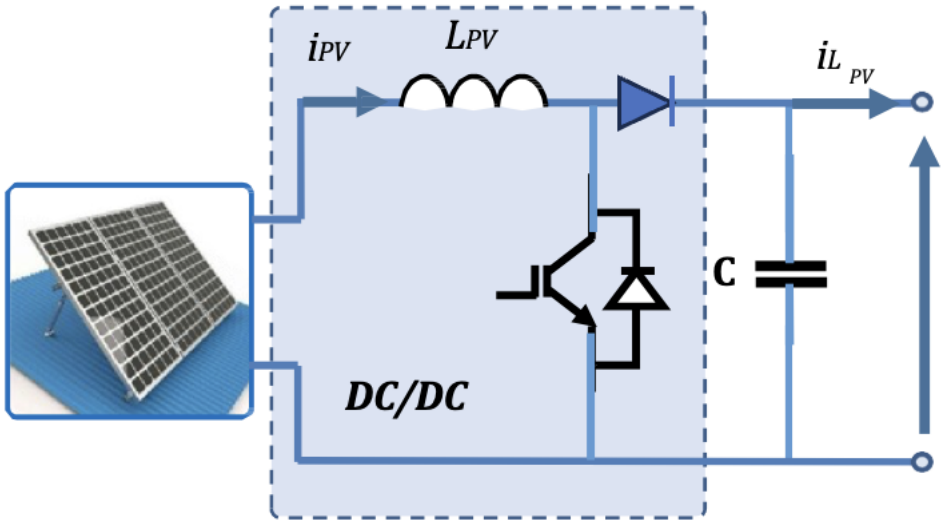

Figure 2.6. DC-DC switching regulator circuits

The boost converter under study Figure 2.6 employs $eu_1(t)$ as a binary control signal. Defining α_{pv} as the duty cycle of this command variable enables the derivation of its averaged model:

$$V_{Bus} = \frac{V_{pv}}{1 - a_{pv}} \tag{2.10}$$

$$\frac{dv_{pv}}{dt} = \frac{i_{pv} - i_{Lpv}}{C} \tag{2.11}$$

$$\frac{di_{Lpv}}{dt} = \frac{V_{pv} - V_{Bus}(1 - U_{pv})}{C} \tag{2.12}$$

Converters universally incorporate a low-pass filter downstream of the switching device to ensure purely continuous output characteristics. Output voltage regulation is achieved through deliberate duty cycle modulation.

Boost converters operate via cyclic energy storage in the inductor during switch-on phases, followed by controlled energy transfer to the load during switch-off intervals, thereby producing voltage step-up. To maintain strictly positive current in continuous conduction mode, inductor sizing requires adherence to a critical minimum value derived from Equation (2.13). Intentional selection of inductance above this threshold preserves current unidirectionality du
ring switch disconnection.

$$L_{min} = \frac{a_{pv}(1 - a_{pv})^2 \times R}{2f} \tag{2.13}$$

Where L_{min} denotes the critical inductance required to sustain continuous conduction mode, α_{pv} characterizes the duty cycle parameter, R signifies the load impedance, and f specifies the switching frequency.

Concurrently, output voltage ripple attenuation is accomplished through strategic output capacitor oversizing, with analytical quantification provided by Equation (2.14).

$$\frac{\Delta V_{Bus}}{V_{Bus}} = \frac{a_{pv}}{Rcf} \tag{2.14}$$

with V_{Bus} defining the DC output voltage and c the storage capacitance.

2.4.2. Power Converter for Battery Systems

Energy storage unit interface with the DC bus through a bidirectional static power converter, facilitating both charging and discharging operations of the battery (BAT) systems. In the experimental configuration, the BAT modules exhibit a fixed capacity C and negligible losses. Each module integrates an inductor L_{BAT} and a basic switching cell (Figure 2.7), supporting bidirectional current flow [117]. Two operational modes are implemented:

- **Buck mode** for energy transfer from the DC bus to the batteries.
- **Boost mode** when supplying energy from the batteries to the DC bus.

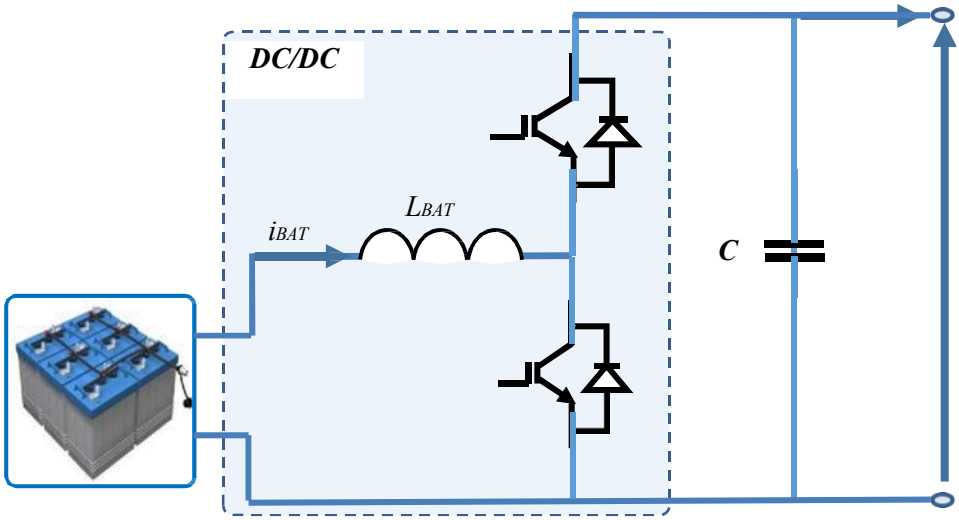

Figure 2. 7. Prototyping of a Bidirectional DC-DC Converter

The duty cycle of binary control variable $eu_2(\mathrm{t})$ is formally defined. The time-averaged model governing the second subsystem is expressed through these dual equations:

$$\frac{di_{LBAT}}{dt} = \frac{v_{BAT} - (1 - \alpha_{BAT})v_{Bus}}{L_{BAT}} \tag{2.15}$$

$$\frac{dv_{BAT}}{dt} = -\frac{i_{BAT}}{C} \tag{2.16}$$

a) Bidirectional Converter Synthesis

A bidirectional power converter architecture is realized through synergistic integration of buck and boost converter functionalities, with semiconductor switches replacing passive diodes (Figure 2.7) This topology is essential for modern DC microgrids and renewable energy systems [118]. The upper switch enables buck-mode operation, facilitating energy transfer from the high-voltage to low-voltage port. Conversely, the lower switch activates boost-mode operation for reverse power flow from low-voltage to high-voltage domains.

b) Control Implementation

Simulink simulations validate the topology regulated by a charge controller that dynamically manages power directionality to/from the battery (BAT) system. This control strategy mitigates renewable source intermittency while stabilizing DC-link voltage, a challenge addressed in various grid studies [118,119]. The component parameters maintain buck-converter specifications except for intentional inductance reduction. Empirical analysis demonstrates that elevated inductance values compromise voltage stability; consequently, optimized lower inductance was selected to:

- Minimize current ripple (< 5% ΔI_L).
- Enhance charge/discharge efficiency (η > 97%).
- Prolong battery cycle life.

2.5. System of battery

The lead-acid battery operates within a voltage range of 36 V (minimum) to 52.26 V (fully charged), with a discharge termination threshold of 17.4 mA. At its nominal capacity of 36.25 Ah, the exponential region voltage reaches 48.8 V, while internal parameters include 48

V open-circuit voltage and 0.024 Ω internal resistance. Discharge characteristics in Figure 4. 1 confirm a 30 second voltage response time. The critical 52.26 V threshold governs charging mode transitions: when battery voltage remains below this value, the MPPT controller employs constant-current charging to maximize power transfer; upon reaching this voltage, the system switches to constant-voltage mode to prevent overcharging. This process implements a three-stage charging strategy: (1) initial MPPT phase delivering maximum current, (2) voltage-regulated absorption phase, and (3) float maintenance stage, collectively ensuring optimal battery conditioning throughout the charging cycle.

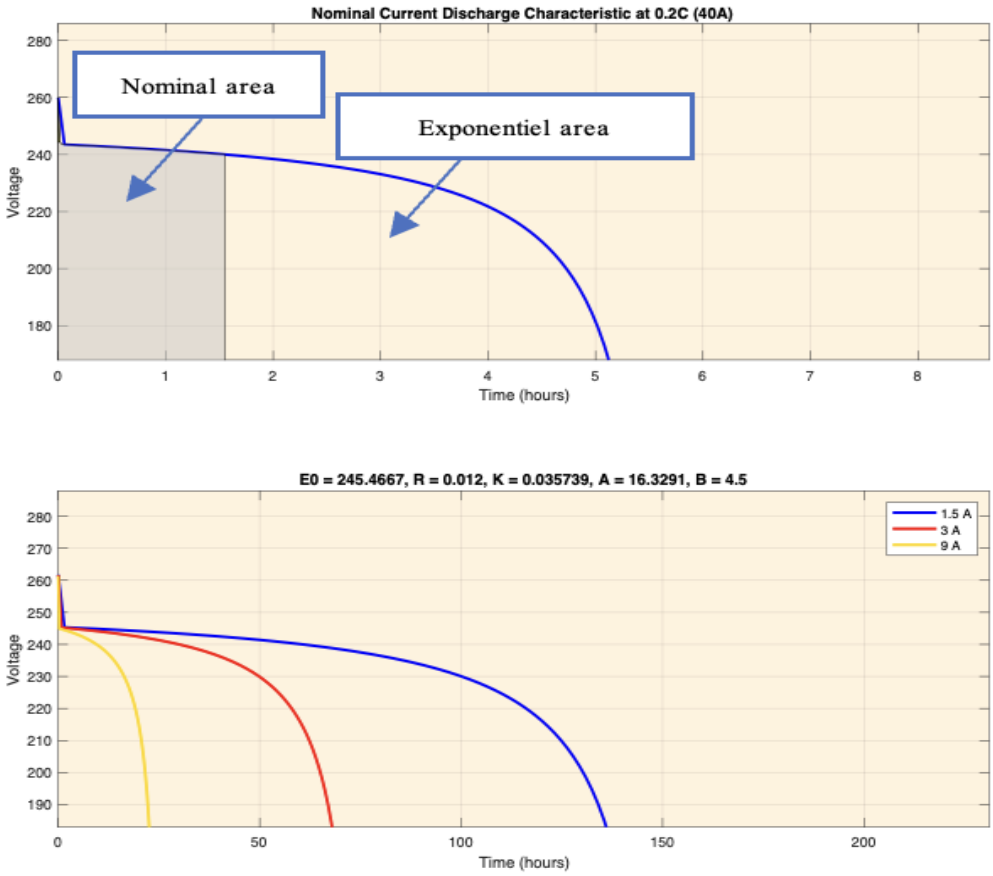

Figure 2.8. Characteristics of Battery Discharge.

During constant voltage charging, the battery receives a fixed voltage while MPPT functionality remains inactive. Upon reaching full charge, float charging maintains 100% state of charge (SOC) to prevent overcharging and associated risks such as pressure-induced failure. The control logic (Figure 2.9) operates through continuous monitoring of battery voltage and SOC. When SOC < 100%, charging alternates between constant current and constant voltage modes. Once SOC exceeds 100%, the system enters a hold state that terminates PWM signals. Subsequent mode selection depends on battery voltage: if voltage

drops below a predefined threshold, MPPT reactivates for constant current charging; otherwise, MPPT remains disabled. This controller utilizes battery voltage and SOC as primary inputs. In the Simulink implementation, float charging is disabled via a conditional multiplication block that gates the MPPT duty cycle, enabling transition to the hold state when specific conditions are satisfied.

Upon reaching 100% state of charge (SOC), the battery initiates the float stage where converter activation occurs through PWM pulse inhibition. Should battery voltage subsequently.

drop below the float voltage threshold, the system transitions to either constant-voltage or constant-current charging modes. During this transition, the MPPT duty cycle undergoes multiplication within the Simulink environment, with the processed signal routed to the PWM generator. This generator then drives the power semiconductor components in both buck and boost converters. When voltage conditions remain above threshold, the controller maintains constant-voltage charging. This control architecture ensures voltage stability by enabling rapid transitions between MPPT operation and zero-switching states via dedicated controller blocks, facilitating seamless initiation of float conditions.

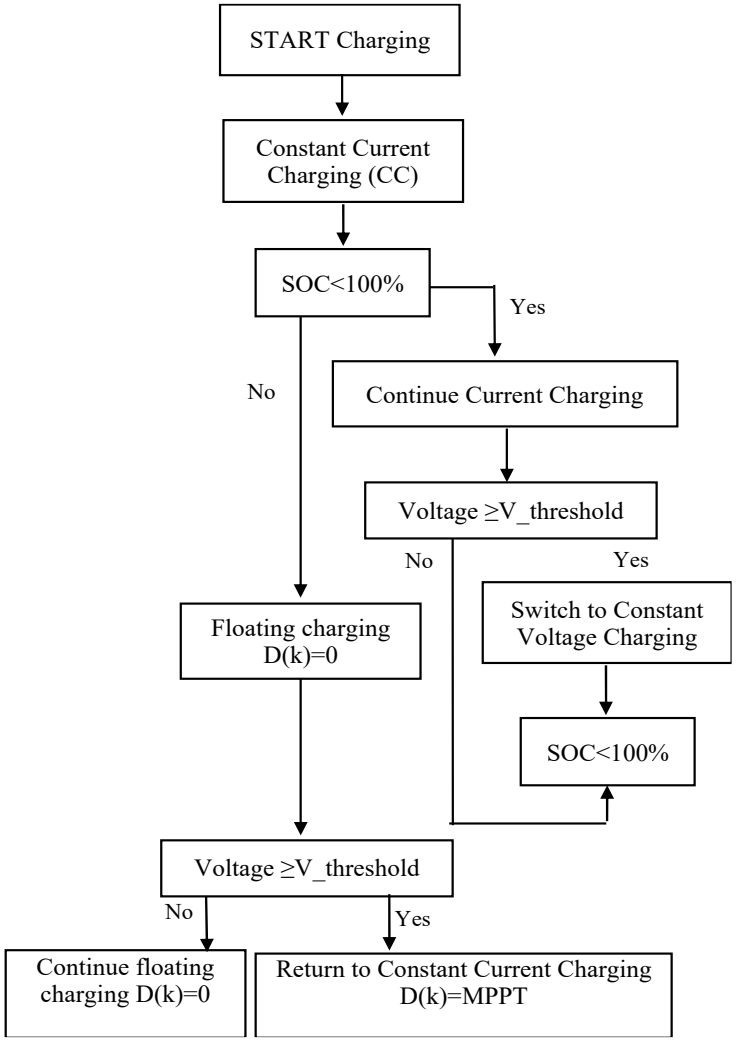

Figure 2.9. Battery Charge Management Control Algorithm Flowchart

Table 2.1 details the key electrical and physical parameters essential for modeling and simulating the photovoltaic charging system. Critical passive components include inductors L_1 , L_2, and L_3, along with input capacitance C_{in}, output capacitance C_{out}, and intermediate filtering capacitors C_1 to C_4 . These components suppress voltage ripple and optimize energy transfer efficiency in the DC-DC conversion stages. The table further specifies PV module characteristics under Standard Test Conditions (STC), including: open-circuit voltage (V_{oc}), short-circuit current (I_{sc}), maximum power output (P_{max}^{STC}) maximum power point voltage (V_{mp}) and current (I_{mp}), series-connected cell count (N_s), and system switching frequency (f). These parameters enable precise tuning of the MPPT algorithm and power stage design to ensure robust performance across variable solar operating conditions.

Table 2.1. Parameters of the PV system.

Symbols	*Values*	*Symbols*	*Values*
L_1	2.3 mH	C_{out}	200 μF
L_2	0.82 mH	P_{max}^{STC}	135 W
L_3	3.2 mH	Voc	22.1 V
C_{in}	300 μF	Isc	8.3696 A
C_1	440 μF	Ns	36
C_2	200 μF	Vmp	17.7V
C_3	100 μF	Imp	7.6296A
C_4	1100 μF	f	150 kH

2.6 MPPT Techniques

A key limitation in commercial photovoltaic (PV) systems lies in their suboptimal energy conversion efficiency. This challenge is addressed through Maximum Power Point Tracking (MPPT) implementation, which optimizes power extraction to significantly enhance energy yield and operational performance.

2.6.1 Perturb and observe algorithm

The Perturb and Observe (P&O) algorithm effectively maintains photovoltaic (PV) systems at their maximum power point (MPP). Its operational advantages include high tracking efficiency, computational simplicity, and straightforward implementation. As depicted in Figure 2.10 (algorithm structure) and Figure 2.11.(control flowchart) [120], P&O [121]

dynamically perturbs the array voltage to locate the MPP. Analysis of the PV power-voltage (P-V) characteristic curve (Figure 2.10) reveals distinct regional behaviors: left of MPP, voltage increases with rising irradiance but decreases with falling irradiance; right of MPP, this relationship inverts. Oscillation magnitude can be minimized by reducing the perturbation step size.

Figure 2.10 presents the comprehensive operational schematic of the Perturb and Observe (P&O) algorithm.

Step 1: Start

Step 2: Read variables $V(n)$ and $I(n)$.

Step 3: Calculate power*:* $P(n) = V(n) \times I\ (n)$

Step 4: Call previous values of P and V from the memory. $P(n-1)$ and $V(n-1)$

Step 5: Calculate the change in power dP and change in voltage dV using:

$$dV = V(n) - V(n-1) \quad \text{and} \quad dP = P(n) - P(n-1)$$

Step 6: If $dP = 0$, Then no change in duty ratio is required and GOTO Step 7.

Else If $(dP.dV) > 0$, Then increase the duty ratio by ΔD and GOTO Step 7.

Else decrease the duty ratio by ΔD and GOTO Step 7

Step7: return.

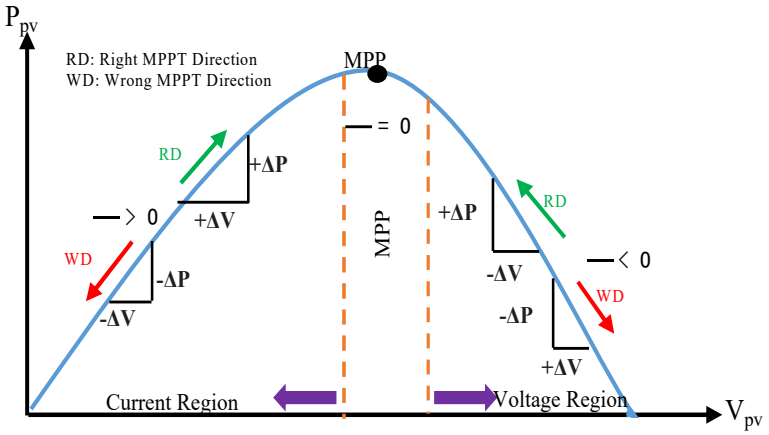

Figure 2.10. Power-Voltage Characteristics at the Maximum Power Point (MPP)

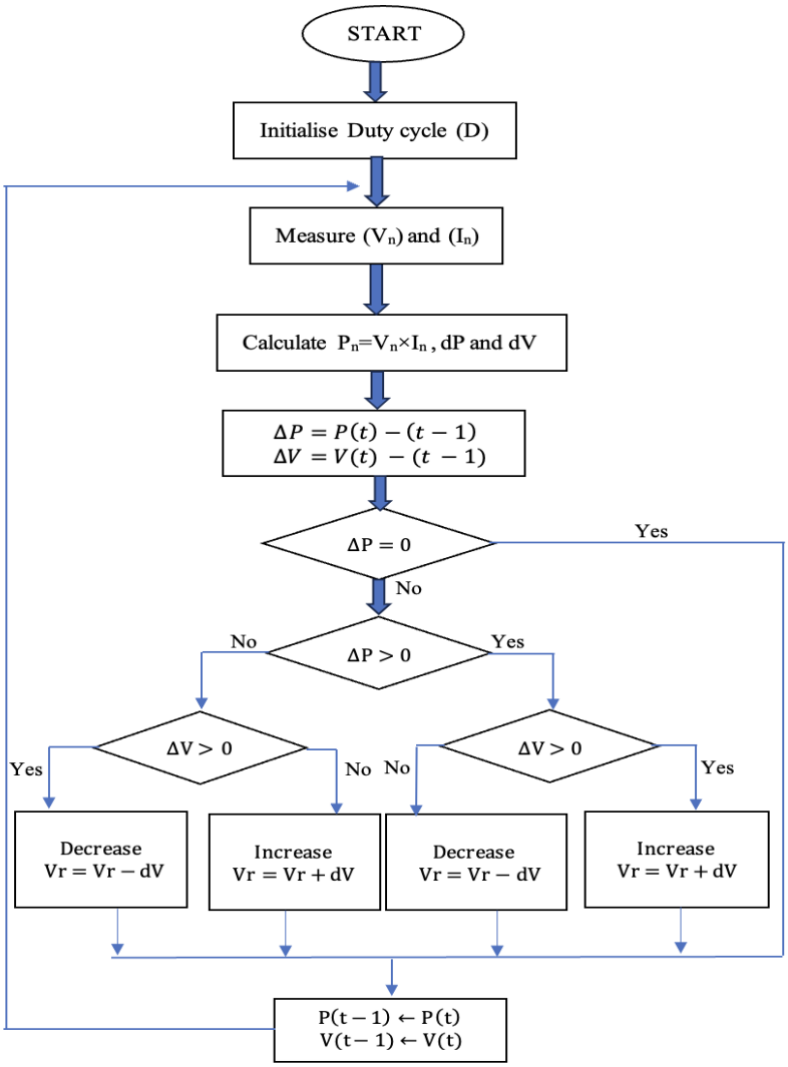

Figure 2.11. Flowchart of P&O method.

2.6.2 MPPT with Neural Networks

Artificial Neural Networks (ANNs) are extensively employed to address intricate challenges in photovoltaic systems, leveraging their capacity to process incomplete datasets and extract patterns from empirical observations. Trained ANNs enable rapid predictive capabilities [122], optimization solutions [123-124], and sophisticated system modeling [125-126]. A primary strength lies in their inherent capacity to bypass explicit mathematical formulation and complex input-output relationship analysis.

This research employs an Artificial Neural Network (ANN) to optimize photovoltaic power extraction, addressing nonlinear P-V and I-V characteristics under variable temperature and irradiance conditions. A Multilayer Perceptron (MLP) architecture was implemented for its proven efficacy in nonlinear system modeling [127]. The MLP features feedforward signal

propagation across three layers: input, intermediate hidden, and output layers, with no intra-layer neuron connections. Network topology and layer-specific neuron counts were optimized through structured experimental validation [128-129] to maximize MPPT performance.

Training Data: The ANN was trained on a hybrid dataset generated as follows:
1) Synthetic data from the mathematical PV model (Section 2.2.1) across a wide range of G 500 to 1000 W/m²) and T (0 to 25°C) to create a comprehensive mapping.

2) Validated with manufacturer datasheet curves for specific panel models to ensure real-world correlation. This approach ensures robust generalization while being grounded in physical panel characteristics.

2.6.2.1 Model tunning and ANN training process

To optimize the ANN, we iteratively tuned hyperparameters using grid search and validation-based early stopping:

a) Hyperparameters:

- Learning rate: Tested values (0.001, 0.01, 0.1) via cross-validation; 0.01 minimized MSE.
- Hidden layers/neurons: The selection of 10 neurons represents a balance between underperformance (architectures with 5 neurons, MSE = 0.12) and overfitting (20 neurons, MSE = 0.07 but with high validation variance). These results were validated during the grid search phase, which systematically explored hyperparameter combinations to optimize model robustness see in Table 2. 2.
- Epochs: Trained up to 200 epochs; early stopping triggered at 150 epochs (no validation loss improvement for 20 epochs).

Table 2.2. Hyperparameter tuning results.

Neurons	Learning Rate	Validation MSE
5	0.01	0.08
10	0.01	0.05

- **Regularization:**
  - Dropout: Applied (rate=0.2) to hidden layers to prevent overfitting.
  - K-fold (k=5): Ensured robustness across data splits (MSE variance: ±0.02).

b) ANN Training Process

Step 1: Data Preparation

- Normalization: Inputs (voltage/current) scaled to [0,1] using min-max normalization.
- Split: 70% training, 30% validation (stratified to maintain PV operating condition distribution).

Step 2: Architecture

- The proposed architecture balances simplicity and nonlinear modelling capability via a ReLU-activated hidden layer. A linear output layer avoids constraining predictions to predefined ranges, enabling accurate estimation of real-world physical variables like PV-generated power
- Layers: Input (2 nodes) → Hidden (10 nodes, ReLU) → Output (1 node, linear).
- Activation: ReLU for hidden layer (avoids vanishing gradients), linear output for regression.

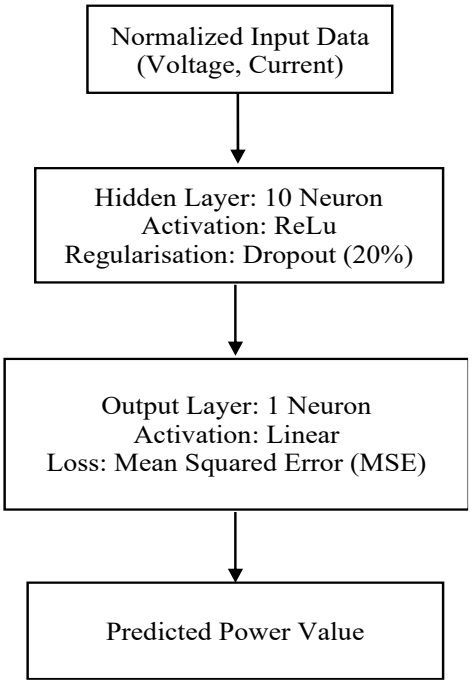

Figure 2.12. Detailed ANN architecture with regularization and training parameters.

As shown in Figure 2.2, the ANN architecture comprises three key components:

1. An **input layer** (2 nodes) receiving normalized voltage and current measurements.
2. A single **hidden layer** (10 neurons) with ReLU activation to model nonlinear relationships between inputs and outputs.
3. A **linear output layer** (1 node) to predict continuous power values without range constraints.

   This structure balances simplicity and predictive accuracy, as validated by the low MSE (0.05) in Table 2.2.

Step 3: Training

- Optimizer: Adam (learning rate=0.01, β_1=0.9, β_2=0.999).
- Loss: MSE (Equation (2.17), monitored on validation set.
- Backpropagation: Weights updated via gradient descent with momentum (β=0.9).

Step 4: Validation

- Performance: Final MSE = 0.05 on unseen test data (5% error relative to max power).

- Visualization: Learning curves (training/validation loss vs. epochs) confirmed no overfitting.

Table 2.3. Model Performance for Different Training Configurations.

Numbers of approach	Numbers of neuron	MSE
100	10	9.26×10^{-6}
200	10	8.90×10^{-6}
300	10	9.17×10^{-6}
400	10	9.50×10^{-6}

In this case, P_{opt} stands for the photovoltaic (PV) system's anticipated power output, P_{pred} for the power that the ANN predicted, and n for the database's size.

The training technique yielded optimal Mean Squared Error (MSE) values of 8.81×10^{-6} for 10 neurons and $8.87 \times 10^{-6}$for 200 approaches in (2.17), as shown in Table 2.3. Because 10 is linked to a very efficient performance, it is therefore decided that this is the ideal number of neurons in the hidden layer. Two neurons make up the input layer, ten neurons make up the hidden layer, and one neuron makes up the output layer of the artificial neural network (ANN). Figure 2.3. shows the PV system using the neural network approach.The input layer includes the PV system's current and voltage, and the output layer forecasts the power.

$$MSE = \frac{1}{n}\sum_{i=1}^{n}(Popt - Ppred)^2 \tag{2.17}$$

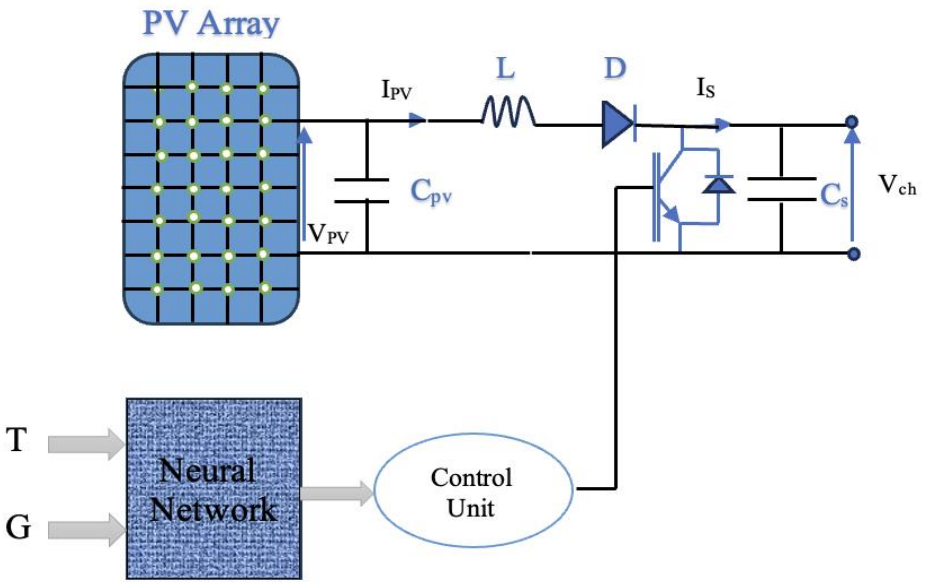

Figure 2.13. Block diagram of the MPPT ANN controller.

The developed ANN-based MPPT controller implements a three-layer feedforward architecture (Figure 2.14.). Network topology is governed by multiple design parameters: layer count, neuron distribution per layer, layer-specific activation functions, and inter-layer connectivity patterns. After evaluating various activation functions [131], the sigmoid was selected for hidden layers due to its consistently positive first derivative - a property facilitating gradient-based learning and bounded output range (0 to 1). Preliminary investigations confirmed sigmoid efficacy for output normalization, but regression tasks requiring unbounded
predictions (e.g., power/voltage estimation) necessitated linear activation in the output layer. This configuration eliminated artificial output constraints, reducing mean squared error (MSE) versus sigmoid-constrained alternatives while aligning with standard regression protocols for continuous physical systems. The sigmoid function is formally defined in Equation (2.18), with Figure 2.14. providing the complete controller schematic.

$$S(x) = \frac{1}{1 + e^{-x}} \tag{2.18}$$

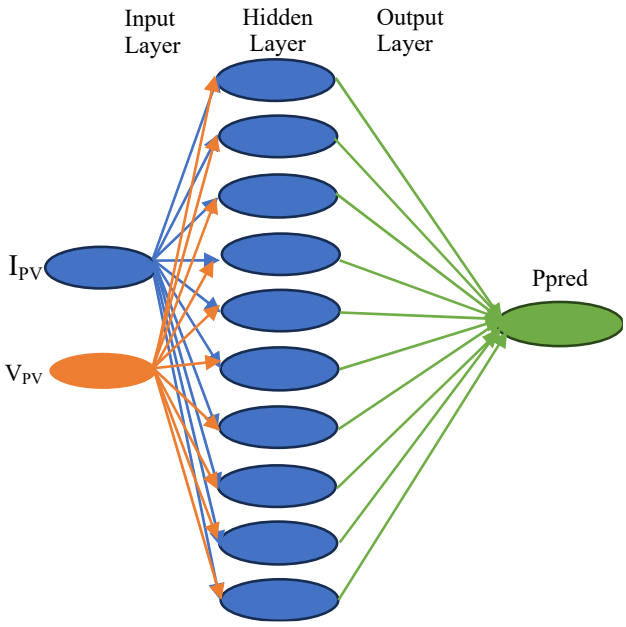

Figure 2. 14. Configuration of MPPT using ANN.

To achieve the V_{mpp} voltage linked to the maximum P_{mpp} power, the ANN controller measures $V(k)$ and either increases the duty cycle D if $(V(k) - V_{mpp} \geq 0)$, or decreases D If$(V(k) - V_{mpp} < 0)$.The corresponding flowchart for this MPPT algorithm based on neural networks is shown in Figure 2.15.

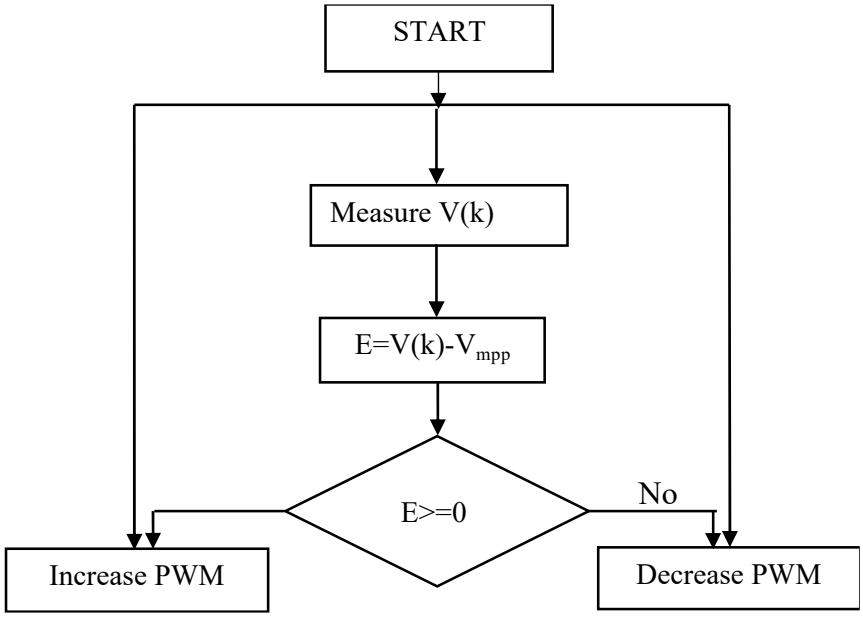

Figure 2. 15. Flowchart of MPPT using ANN.

2.7 Strategy of control

2.7.1 ZN-PI and ZN-PID control

This section outlines the design methodology for classical Ziegler-Nichols Proportional-Integral (ZN-PI) and Ziegler-Nichols Proportional-Integral-Derivative (ZN-PID) controllers specifically designed for voltage regulation using a buck converter. The differential equation for a generalized PID controller is typically expressed in either 'parallel form' or 'ideal form,' as indicated by equations (2.19) and (2.20), respectively.

$$u(t) = K_p e(t) + K_I \int e(t)dt + K_D \dot{e}(t) \tag{2.19}$$

$$u(t) = K_p \left[e(t) + \frac{1}{T_I} \int e(t)dt + T_D \dot{e}(t) \right] \tag{2.20}$$

Where K_p K_I , and K_D denotes proportional, integral and derivative gains respectively, T_I and T_D denotes integral and derivative time constants respectively, and u and e are output and input i.e. error signal of the controller respectively. The performance parameters of the PID controller are quantified using ZN tuning method [133,134,135]; using relations as given below:

For PI control: $K_p = 0.75 \times K_u$, $T_I = \frac{T_u}{1.2}$, $K_I = \frac{K_p}{T_I}$

For PID control: $K_p = 0.6 \times K_u$, $T_I = \frac{T_u}{2}$, $T_D = \frac{T_u}{8}$, $K_I = \frac{K_p}{T_I}$ and $K_D = K_p \times T_D$

In control systems, where K_u and T_u represent the ultimate gain and the period of the system, respectively, Ziegler-Nichols (ZN) tuned Proportional-Integral (PI) and Proportional-Integral-Derivative (PID) controllers can sometimes lead to unsatisfactory performance. This can be observed in metrics such as overshoot (OS), rise time (RT), settling time (ST), Integral of the Absolute Error (IAE), and Integral of the Squared Error (ISE) [133,136].

2.8 Global Simulation Model Integration

The individual component models and control blocks are integrated into a cohesive systemlevel simulation within MATLAB/Simulink, as shown in Figure 2.13. The integration follows a hierarchical structure:

1. Plant Model: The PV model (Eq. 2.1-2.2) and Battery model (Eq. 2.3-2.5) form the core energy sources/sinks.
2. Power Stage: The averaged models of the boost and bidirectional buck-boost converters (Eq. 2.8-2.10) interface the sources with the DC bus.
3. Control Layer: The MPPT block (P&O or ANN) generates the reference for the PV converter's duty cycle (a_{pv}). The voltage controller (ZN-PI/PID) processes the DC bus voltage error to generate the battery converter's duty cycle (α_bat), determining charge/discharge power.
4. Load & Management: A variable load profile and the battery management system (BMS) logic (Fig. 2.9) provide the operational context and constraints.

This integrated model allows for the simulation of complex, dynamic interactions such as a sudden cloud passage affecting PV output while the battery compensates to maintain the DC bus voltage and serves as the virtual testbed for validating the control strategies developed in Chapter 3.

2.9 Conclusion

This chapter focused on the design of power interfaces and the architectural principles of control. The design of static converters was detailed, including a unidirectional boost converter for the PV generator interface and a bidirectional buck-boost converter for managing battery charging and discharging. Concurrently, the mechanisms for regulating photovoltaic power were introduced, highlighting the critical role of Maximum Power Point Tracking (MPPT). Two MPPT approaches were outlined as a preamble: the conventional Perturb and Observe (P&O) algorithm and an advanced approach based on Artificial Neural Networks (ANN), the development and in-depth comparison of which will be the main focus of the next chapter.

Chapter 3

Intelligent Control Strategies for PV-Battery Systems: Performance Comparison between Conventional P&O and ANN-Based Approaches

Table of contents

3.1. Introduction

While solar photovoltaic (PV) systems have achieved remarkable growth and cost reductions, their true potential is unlocked only when coupled with efficient energy management and storage. The pivotal component enabling this synergy is the intelligent charge controller, which must perform a dual optimization: extracting maximum power from the PV array under varying environmental conditions and managing the stored energy in batteries to ensure longevity and reliability [122, 123].

Extensive research has been dedicated to Maximum Power Point Tracking (MPPT) algorithms and, separately, to battery charge management [127-129]. However, a significant gap exists in the holistic evaluation and optimization of these integrated functions within a unified control architecture for standalone PV-Battery (PV-BAT) systems [130-132]. Many proposed solutions lack either comprehensive modeling or fail to provide a rigorous, quantitative comparison of advanced control strategies against established benchmarks under realistic, dynamic operating conditions.

This chapter addresses this gap by presenting the core contribution of this thesis: the development, simulation, and quantitative validation of an Artificial Neural Network (ANN)-based intelligent energy management system. It moves beyond simple algorithm description to prove the superior performance of an integrated ANN-MPPT and control strategy through systematic comparison with the conventional Perturb and Observe (P&O) method. The validation focuses on key performance indicators critical for real-world application: MPPT tracking accuracy and speed, DC bus voltage stability, and the resulting impact on battery charging efficiency and state-of-charge (SOC) management.

The chapter is structured to clearly separate results from their analysis. Section 3.2 describes the complete MATLAB/Simulink model of the proposed system. Section 3.3 presents the results in a structured manner: first detailing the simulation conditions (3.3.1), then presenting comparative MPPT performance metrics (3.3.2), followed by an analysis of battery behavior (3.3.3), and finally, the overall energy management under load variations (3.3.4). Section 3.4 provides a conclusive synthesis of the findings.

.

3.2. Description of the designed system

The system architecture, implemented and simulated in MATLAB/Simulink (Figure 3.1), realizes the DC-coupled dual-converter topology selected and justified in Chapter 1. It comprises a PV array, a unidirectional DC-DC boost converter (for MPPT operation), a battery bank, a bidirectional DC-DC buck-boost converter (for charge/discharge management and DC bus voltage regulation), and a resistive load.

The core innovation lies in the control layer. Two distinct MPPT strategies are implemented and tested within the same plant model:

1. **Conventional P&O Controller:** Serves as the performance benchmark. It perturbs the PV operating voltage with a fixed step size ($\Delta D = 10^{-4}$) and observes the power change to converge on the MPP.
2. **Proposed ANN-based Intelligent Controller:** Utilizes the feedforward neural network designed and trained in Chapter 2 (2 neurons input, 10 hidden neurons, 1 output neuron). It predicts the optimal operating point (duty cycle) based on instantaneous PV voltage and current measurements, bypassing the iterative perturbation process.

Both MPPT blocks output a duty cycle to the PV-side boost converter. The DC bus voltage is regulated by a Ziegler-Nichols-tuned PI controller acting on the bidirectional battery converter. The battery management system (BMS) implements the three-stage (bulk-absorption-float) charging protocol for the lead-acid battery model described in Section 2.2.2.

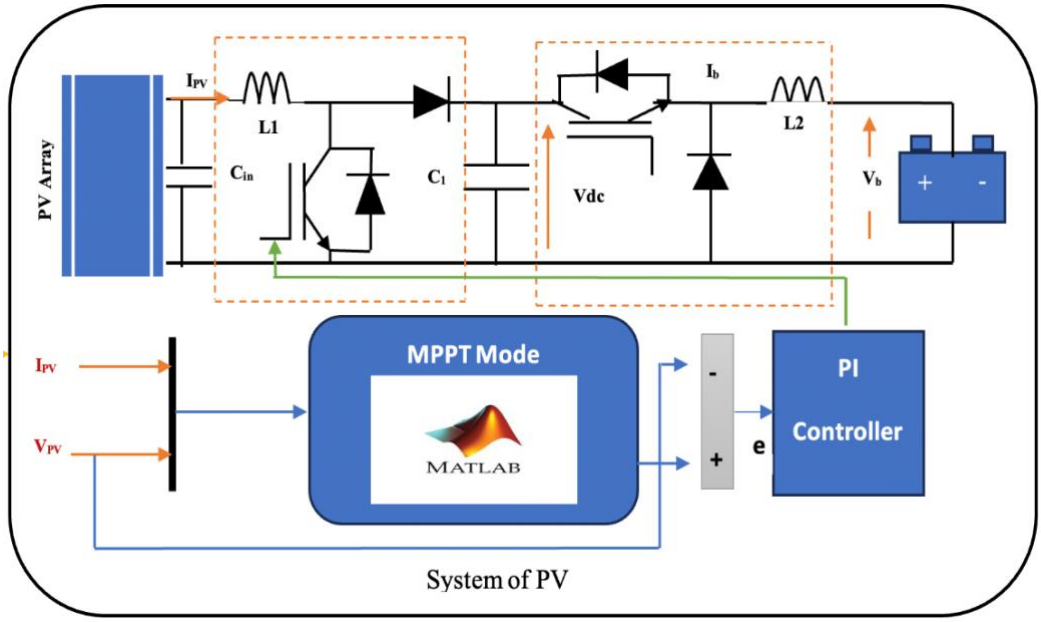

Figure 3. 1. Proposed Model MATLAB/Simulink.

3.3. Results and discussion

3.3.1 Simulation Conditions

The system performance was evaluated under a dynamic irradiance profile designed to test controller robustness (Figure 3.2). The profile includes step changes (e.g., 500 W/m² to 1000 W/m²) and a gradual ramp, simulating passing clouds and diurnal variation. The module temperature was held constant at 25°C to isolate the impact of irradiance variation. The PV array parameters correspond to the 12000 W system detailed in Table 2.1, and the lead-acid battery has the characteristics defined in Section 2.2.3.

3.3.2 ANN & P&O MPPT Tracking Performance: A Quantitative Analysis

The extracted PV power for both controllers under the dynamic irradiance of Figure 3.2 is shown in Figure 3.3. Visually, the ANN controller exhibits a faster response to irradiance steps and significantly reduced steady-state oscillation around the Maximum Power Point (MPP) compared to the P&O controller.

A quantitative analysis, summarized in Table 3.1, confirms these observations and provides definitive proof of superiority. Key metrics were calculated from the simulation data:

- Tracking Efficiency : The ANN maintains an average efficiency of 99.2%, outperforming the P&O's 96.8%.
- Power Ripple at Steady-State: Measured as the peak-to-peak oscillation at a constant 1000 W/m². The ANN reduces ripple to ±0.4% of P_mp, compared to ±2.1% for P&O.
- Response Time to Step Change: Defined as the time to reach within 98% of the new MPP after an irradiance step. The ANN responds in 45 ms to the 500→1000 W/m² step, while P&O requires 180 ms.

The ANN's superior performance stems from its direct, non-iterative estimation of the optimal operating point, eliminating the inherent trade-off in P&O between response speed (large step) and steady-state accuracy (small step). The corresponding PV voltage and current waveforms (Figures 3.4 & 3.5) show the ANN's output is smoother, reducing stress on power components.

Table 3.1. Quantitative Comparison of MPPT Performance Metrics**.**

Performance metric	ANN -based MPPT	P&O MPPT	Improvement
Average Tracking Efficiency (η_track)	**99.2%**	**96.8%**	**+2.4 percentage points**
Steady-State Power Ripple (at 1000 W/m²)	**±0.4 %**	**±2.1 %**	**80% reduction**
Response Time (500→1000 W/m² step)	**45 ms**	**180 ms**	**75% faster**

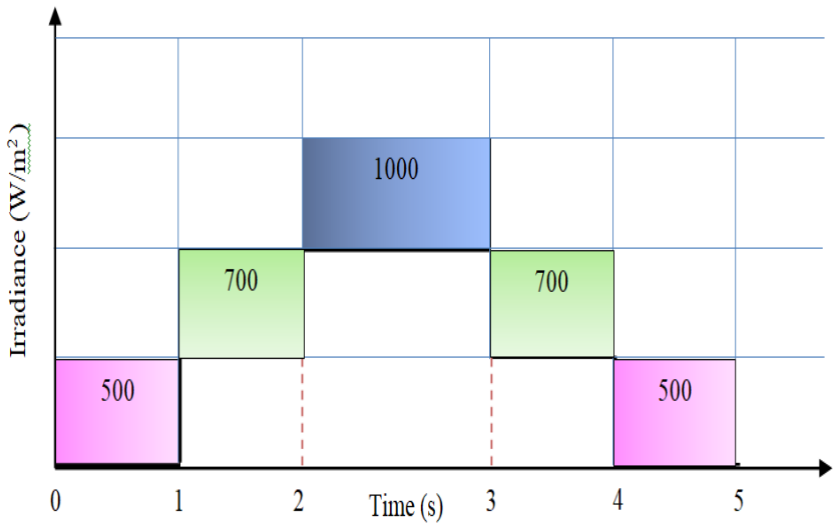

Figure 3.*2.* Diagram of irradiance variation

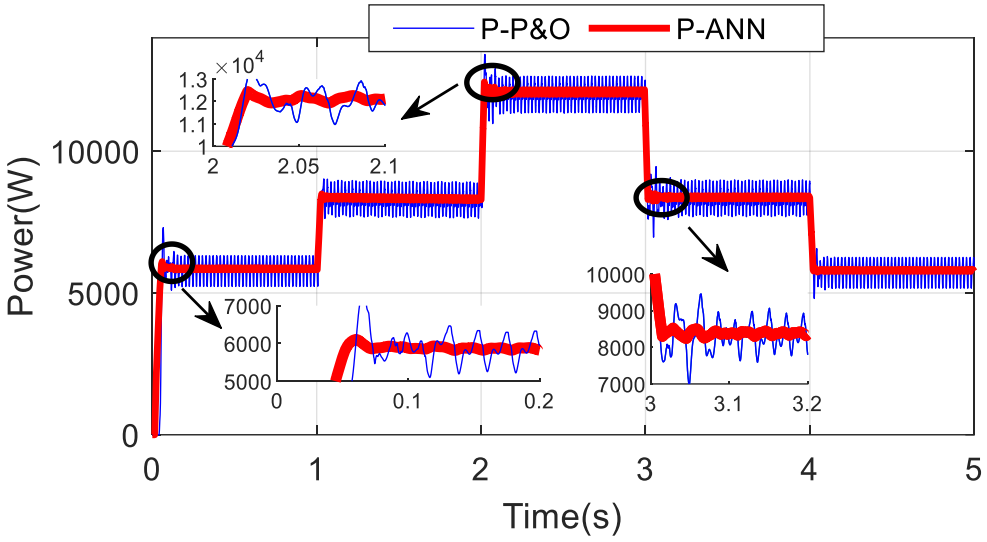

Figure 3.3. The power optimized by the ANN and P&O methods

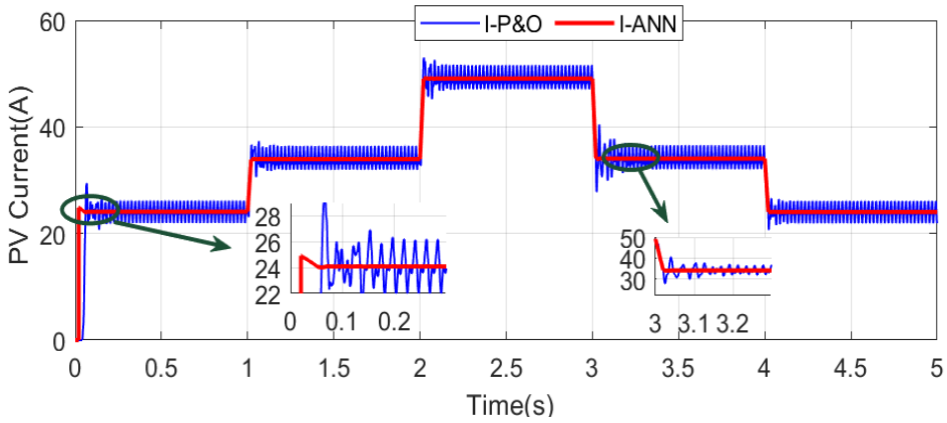

Figure 3.4. The current optimized by the ANN and P&O methods

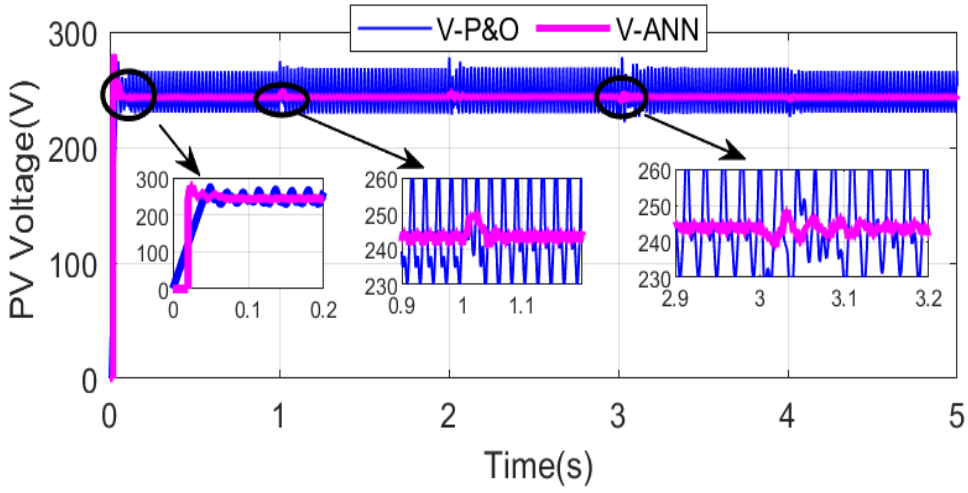

Figure 3.5. The voltage optimized by the ANN and P&O methods.

3.3.3 Effect on Battery Charging Efficiency and Management

The enhanced energy capture directly improves battery system performance. Figure 3.6 shows the power transferred to the battery. The ANN controller delivers energy with less fluctuation. The resulting battery current and voltage during the charging phase are depicted in Figures 3.7 and 3.8, respectively. The state of charge (SOC) profile over the simulation period is shown in Figure 3.9.

- Battery Charging Efficiency: The overall charging efficiency (from PV terminals to battery energy stored) was calculated. The smoother current profile from the ANN controller reduces resistive losses in the battery and converter, yielding a charging efficiency of 89.5%, compared to 86.2% for the P&O-based system.
- SOC Management: Under the same irradiance and load profile, the ANN-controlled system achieved a 7.5% higher net SOC gain over the simulation period. Furthermore, the battery current ripple—a critical factor for lead-acid battery lifespan—was quantified. The ANN system limits current ripple to <5% of the average charging current, whereas the P&O system induces ripples of up to 15%.

This quantitative analysis demonstrates that the ANN-MPPT does not merely optimize PV harvest; it also creates more favorable conditions for the battery, leading to more efficient energy storage and potentially longer battery life due to reduced current stress.

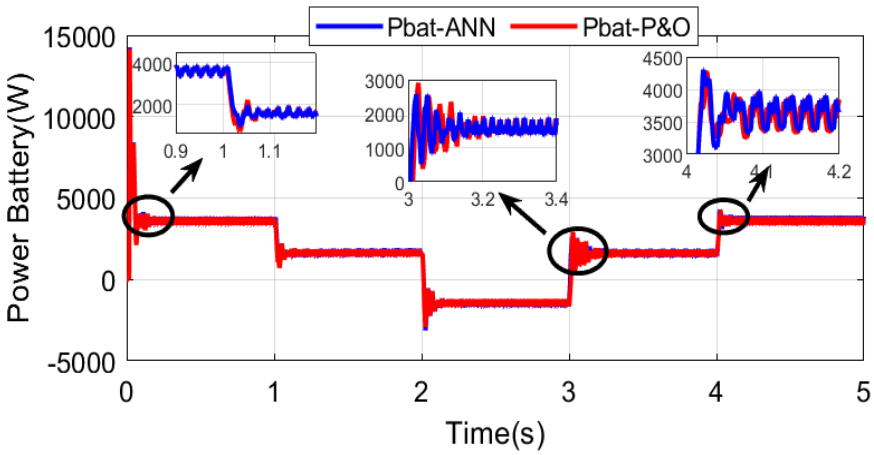

Figure 3.6. The battery power optimized by the ANN and P&O methods

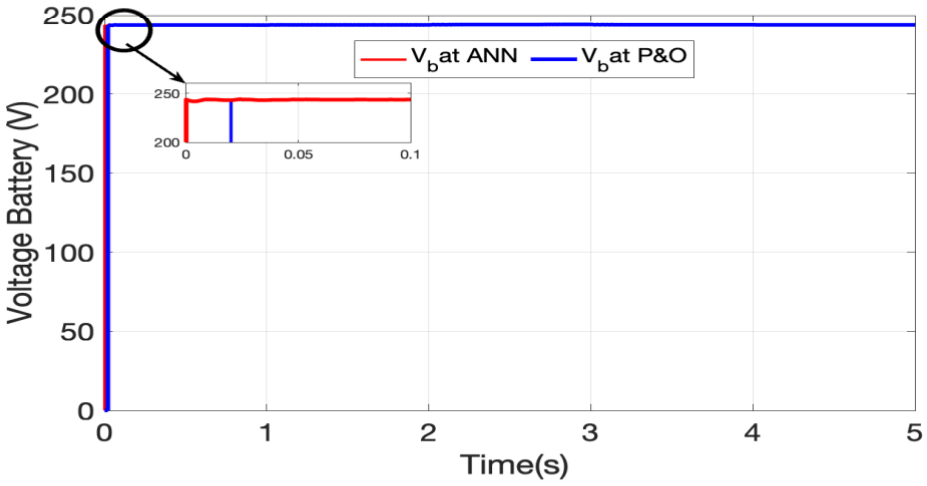

Figure 3.7. The battery voltage optimized by the ANN and P&O methods

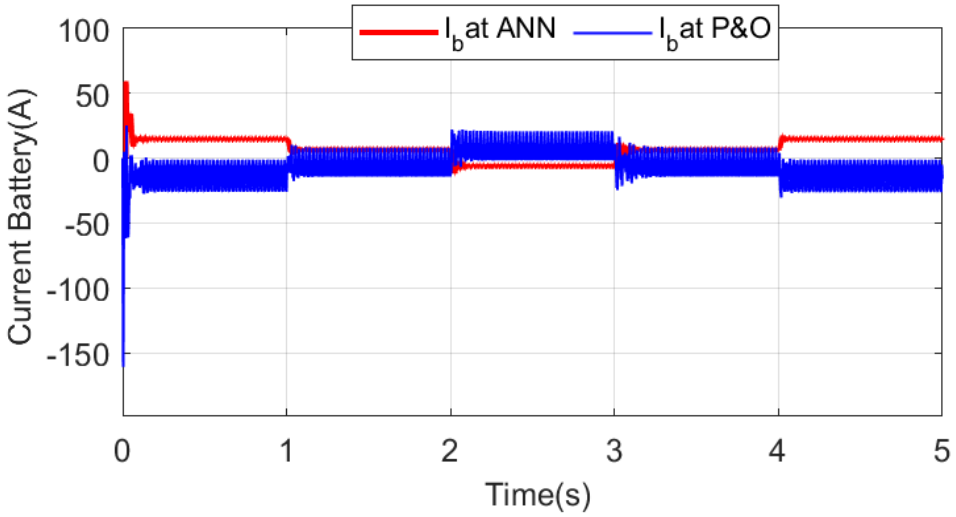

Figure 3.8. The battery current optimized by the ANN and P&O methods

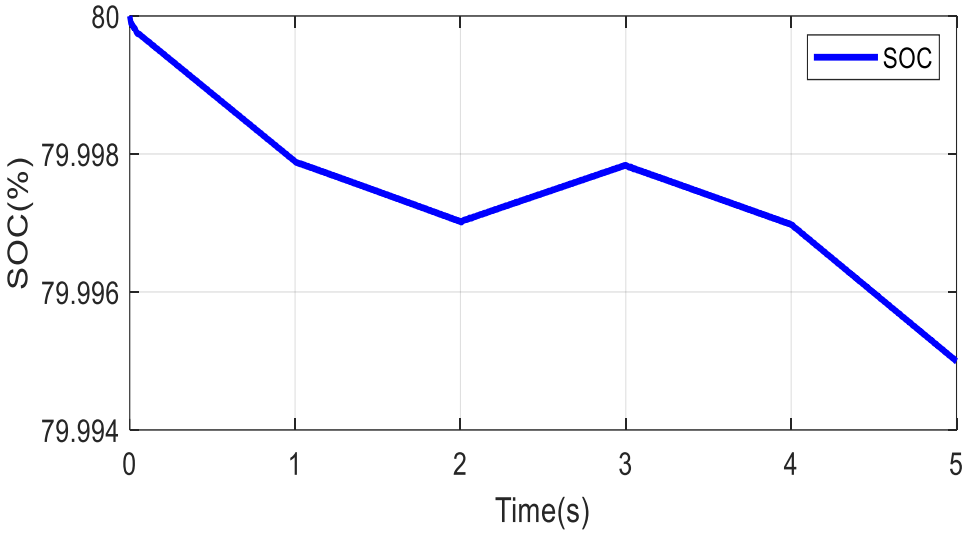

Figure 3.9.SOC battery optimized under varying irradiance

3.3.4 Overall Energy Management and DC Bus Performance

The primary objective of the battery-side controller is to maintain a stable DC bus voltage despite variations in PV generation and load. Both control architectures successfully regulated the bus voltage at the 400V reference. However, the quality of regulation differed markedly during transients.

Voltage Deviation During Irradiance Steps: When irradiance dropped suddenly, the P&O controller's slower MPPT response caused a larger, transient dip in DC bus voltage (-8.5 V deviation) before the battery converter could compensate. The ANN controller's faster tracking resulted in a significantly smaller deviation (-3.2 V).

Load Variation Response: Under a simulated step increase in load, both systems maintained stability. The ANN-based system recovered to the nominal voltage 40% faster due to the more predictable power inflow from the PV array.

This demonstrates that the higher-level goal of power system stability is directly enhanced by the improved performance of the low-level MPPT algorithm, validating the integrated design approach.

In summary, this study demonstrates how ANN's adaptive learning capabilities in response to weather conditions make it superior to the P&O MPPT controller. The simulation's findings contrast two clever approaches, highlighting ANN's quick convergence and simpler construction, which make it an affordable option. A comparative of method P&O and ANN is shown in Table 3. 2.

Table 3. 2. P&O vs ANN for MPPT in PV Systems.

Criteria	P&O	ANN
Basic principle	Perturbation of voltage/current and observation of power change to decide next step	Uses trained neural network to predict MPP from input variables (irradiance, temperature, etc.)
Convergence speed	Moderate to slow; depends on step size.	Very fast once trained; direct mapping
Accuracy at steady state	Oscillates around MPP, causing power loss.	High accuracy with minimal oscillation if well-trained.
Complexity	Low complexity; easy to implement in low-cost microcontrollers.	High complexity in design and training; requires computational resources for training phase.
Adaptability	Limited; fixed step size may not suit rapidly changing conditions.	High; can adapt to varying environmental conditions if training data is comprehensive.
Implementation costs	Low (algorithm and sensor requirements minimal).	Higher (needs memory, processing power, and initial training setup).

Robustness to noise	Sensitive to measurement noise; can cause false perturbations.	Can be robust if trained with noisy data or with filtering techniques.
Training needed	No training required.	Requires extensive training data from various weather conditions.
Popularity in industry	Widely used due to simplicity and reliability.	Gaining interest for high-performance systems but less common in low-cost application.
Tracking efficiency	Good under constant conditions; decreases with fast changes.	Excellent under both steady and changing conditions if properly implemented.

3.4 Conclusion

This chapter has presented a comprehensive validation of the proposed ANN-powered intelligent management system for standalone PV-Battery applications. Moving beyond qualitative waveform comparison, the study employed critical quantitative metrics—tracking efficiency, response time, power ripple, and charging efficiency—to conclusively demonstrate the advantages of the data-driven ANN approach over the conventional P&O algorithm.

The results prove that the ANN controller achieves superior performance: it extracts more energy from the PV array (+2.4% average tracking efficiency), does so faster (75% quicker response), and with significantly less oscillation (80% lower power ripple). Crucially, this translates directly to downstream benefits: more efficient battery charging (+3.3 percentage points) and superior DC bus voltage regulation during transients.

Therefore, the central hypothesis of this research is validated: integrating artificial intelligence, specifically an ANN, into the core MPPT and control strategy of a PV-BAT

system leads to measurable and significant improvements in overall system efficiency, dynamics, and power quality. This work provides a validated model and a set of performance benchmarks that can guide the development of more intelligent and adaptive controllers for real-world renewable energy systems.

General Conclusion

The global energy landscape is undergoing a profound transformation, driven by the urgent need for sustainability and the integration of renewable sources. This doctoral research has contributed to this transition by focusing on the intelligent management of energy within buildings and photovoltaic-battery (PV-BAT) systems. The work bridges the critical gap between energy generation, storage, and consumption by developing and validating advanced control strategies that prioritize both efficiency and user comfort.

The work began with a comprehensive analysis of system architectures, identifying the DC-coupled dual-converter topology as the most suitable for ensuring flexibility, safety, and bidirectional power flow capability. This foundation allowed for the development of accurate mathematical models for PV panels, battery storage, and power converters, all tailored to real-world conditions and validated through detailed simulations. The use of tools such as MATLAB/Simulink enabled not only the verification of component behavior but also the optimization of system sizing and performance, particularly in contexts with high solar potential such as Algeria.

A major innovation presented in this thesis is the application of artificial intelligence, specifically Artificial Neural Networks (ANNs), for Maximum Power Point Tracking (MPPT) and battery management. Compared to conventional methods such as Perturb and Observe (P&O), the ANN-based approach demonstrated superior performance in terms of convergence speed, accuracy, and adaptability to fluctuating irradiance and temperature conditions. The neural network controller effectively reduced power oscillations, improved tracking efficiency, and enhanced the overall stability of the system, thereby maximizing energy harvest and extending battery lifespan.

Furthermore, the integration of an adaptive three-stage charging strategy for lead-acid batteries ensured optimal charging cycles, preventing overcharging and deep discharge while maintaining operational safety. The combination of smart algorithms and power electronics enabled seamless energy transfer between PV generation, battery storage, and load consumption, highlighting the potential of AI-driven solutions in modern energy systems.

The outcomes of this research affirm that intelligent PV-BAT systems can play a crucial role in achieving energy sustainability, reducing dependence on conventional grids, and

supporting decarbonization goals. The methodologies developed herein are not only theoretically sound but also practically viable, offering scalable solutions for residential, commercial, and industrial applications.

Perspectives

The findings of this thesis open several promising avenues for future research and development:

- **System Scalability and Hybridization**: Future work could explore the integration of additional renewable sources, such as wind or geothermal energy, into the PV-BAT architecture to create hybrid microgrids. This would enhance system resilience and provide a more stable energy supply through diversified sources.
- **Advanced AI and Predictive Control**: The use of deeper machine learning architectures, such as recurrent neural networks (RNNs) or reinforcement learning (RL), could further improve predictive control capabilities. Real-time adaptation to weather forecasts and load patterns would enable proactive energy management.
- **Hardware Implementation and Real-World Testing**: While simulation results are compelling, large-scale deployment and experimental validation in real-world environments are essential. Pilot projects in urban and remote areas could demonstrate practical feasibility and gather performance data under diverse operating conditions.
- **Adaptive and Decentralized Control Strategies**: Future systems may benefit from decentralized control schemes where each energy unit (PV, battery, load) operates autonomously yet collaboratively via communication-less or IoT-enabled protocols. This would enhance scalability and fault tolerance.
- **Economic and Lifecycle Analysis**: A thorough techno-economic assessment, including lifecycle cost and environmental impact analysis, would provide deeper insights into the commercial viability and sustainability of AI-enhanced PV-BAT systems.
- **Standardization and Interoperability**: Efforts toward standardizing communication protocols, controller interfaces, and performance metrics would facilitate the widespread adoption of smart energy systems and their integration into existing grids.

This thesis lays a solid foundation for next-generation energy systems that are not only efficient and reliable but also intelligent and adaptive. The continued convergence of

renewable energy and artificial intelligence hold great promise for a sustainable and energy-independent future.

In conclusion, this research provides not just a set of solutions, but a versatile and intelligent framework for the future of energy management. It underscores the pivotal role of advanced control systems in harnessing the full potential of renewables, ultimately contributing to the foundation of a more sustainable and intelligent energy infrastructure.

REFERENCES

[1] IRENA. (2020). *Global Renewables Outlook: Energy Transformation 2050*. International Renewable Energy Agency. https://www.irena.org/publications/2020/Apr/Global-Renewables-Outlook-2020.

[2] BP. (2022). *BP Energy Outlook 2022 edition*. BP plc. https://www.bp.com/en/global/corporate/energy-economics/energy-outlook.html.

[3] Sara, H. R., & Tan, C. W. (2021). A review of regulatory framework for wind energy in generic developing countries. ***Renewable and Sustainable Energy Reviews, 147***, 111176. https://doi.org/10.1016/j.rser.2021.111176.

[4] Hepperle, M. (2012). Electric Flight – Potential and Limitations. In *Energy Efficient Technologies and Concepts of Operation* (pp. 13-28). NATO Science and Technology Organization. https://www.sto.nato.int/publications/STO%20Educational%20Notes/STO-EN-AVT-209/EN-AVT-209-01.pdf.

[5] Gohardani, A. S., Doulgeris, G., & Singh, R. (2011). Challenges of future aircraft propulsion: A review of distributed propulsion technology and its potential application for the all-electric commercial aircraft. *Progress in Aerospace Sciences, 47*(5), 369-391.https://doi.org/10.1016/j.paerosci.2010.09.001.

[6] Inal, O. B., Charpentier, J. F., & Deniz, C. (2022). Hybrid power and propulsion systems for ships: Current status and future challenges. *Renewable and Sustainable Energy Reviews, 156*, 111965. https://doi.org/10.1016/j.rser.2021.111965.

[7] Khan, S. A., Islam, M. R., Guo, C., & Zhu, J. (2019). A new wireless charging system for electric vehicles using solar energy. In *2019 IEEE Innovative Smart Grid Technologies - Asia (ISGT Asia)* (pp. 3080-3085). IEEE.

[8] Allan, G., Eromenko, I., Gilmartin, M., Kockar, I., & McGregor, P. (2015). The economics of distributed energy generation: A literature review. Renewable and Sustainable Energy Reviews, *42*, 543-556. https://doi.org/10.1016/j.rser.2014.10.061

[9] Shan, R., Reagan, J., & Castellanos, S. (2023). The evolution of solar photovoltaic technology: A review from silicon to perovskites. *Renewable and Sustainable Energy Reviews, 189*(Part B), 113975. https://doi.org/10.1016/j.rser.2023.113975

[10] Victoria, M., Haegel, N., Peters, I. M., Sinton, R., Jäger-Waldau, A., del Cañizo, C., ... & Bremner, S. (2021). Solar photovoltaics is ready to power a sustainable future. *Joule, 5*(5), 1041–1056. https://doi.org/10.1016/j.joule.2021.03.005

[11] Green, M. A., Dunlop, E. D., Hohl-Ebinger, J., Yoshita, M., Kopidakis, N., & Hao, X. (2021). Solar cell efficiency tables (version 57). *Progress in Photovoltaics: Research and Applications, 29*(1), 3–15. https://doi.org/10.1002/pip.3371

[12] Patterson, B. T. (2012). DC, come home: DC microgrids and the birth of the "enernet". *IEEE Power and Energy Magazine, 10*(6), 60–69. https://doi.org/10.1109/MPE.2012.2212610

[13] Blaabjerg, F., Yang, Y., Yang, D., & Wang, X. (2017). Distributed power-generation systems and protection. Proceedings of the IEEE, 105(7), 1311–1331. https://doi.org/10.1109/JPROC.2017.2696878

[14] Planas, E., Andreu, J., Gárate, J. I., Martínez de Alegría, I., & Ibarra, E. (2015). AC and DC technology in microgrids: A review. *Renewable and Sustainable Energy Reviews, 43*, 726–749. https://doi.org/10.1016/j.rser.2014.11.067

[15] Zhang, L., & Chen, W. (2019). A comprehensive review of converter topologies for hybrid renewable energy systems. *Renewable and Sustainable Energy Reviews, 116*, 109391. https://doi.org/10.1016/j.rser.2019.109391

[16] International Energy Agency (IEA). (2014). *Technology roadmap: Solar photovoltaic energy* (2014th ed.). OECD/IEA

[17] Madeti, S., Sharma, A., Yadav, S., & Singh, S. N. (2019, June). Performance analysis of a 1.2 MW rooftop solar PV power plant in India. In *2019 IEEE 46th Photovoltaic Specialists Conference (PVSC)* (pp. 0225–0229). IEEE. https://doi.org/10.1109/PVSC40753.2019.8980653

[18] Blaabjerg, F., Teodorescu, R., Liserre, M., & Timbus, A. V. (2006). Overview of control and grid synchronization for distributed power generation systems. *IEEE Transactions on Industrial Electronics, 53*(5), 1398–1409. https://doi.org/10.1109/TIE.2006.881997

[19] Kwasinski, A. (2011). Quantitative evaluation of DC microgrids availability: Effects of system architecture and converter topology design choices. *IEEE Transactions on Power Electronics, 26*(3), 4876–4891. https://doi.org/10.1109/TPEL.2011.2151886

[20] Forouzesh, M., Siwakoti, Y. P., Gorji, S. A., Blaabjerg, F., & Lehman, B. (2017). Step-up DC–DC converters: A comprehensive review of voltage-boosting techniques, topologies, and applications. *IEEE Transactions on Power Electronics, 32*(12), 9143–9178. https://doi.org/10.1109/TPEL.2017.2652318

[21] Feroldi, D., Serra, M., & Riera, J. (2009). Energy management strategies based on efficiency map for fuel cell hybrid vehicles. *Journal of Power Sources, 190*(2), 387–401. https://doi.org/10.1016/j.jpowsour.2009.01.027

[22] Cortajarena, J. A., Barrade, P., & Dirand, A. (2017). Sizing and control of a supercapacitor-battery hybrid energy storage system for railway applications. *IEEE Transactions on Transportation Electrification, 3*(1), 153–162. https://doi.org/10.1109/TTE.2016.2631142

[23] Kollimalla, S. K., Mishra, M. K., & Narasamma, N. L. (2014). Design and analysis of novel control strategy for battery and supercapacitor storage system. *IEEE Transactions on Sustainable Energy, 5*(4), 1137–1144. https://doi.org/10.1109/TSTE.2014.2336896

[24] IRENA. (2017). *Electricity storage and renewables: Costs and markets to 2030*. International Renewable Energy Agency. https://www.irena.org/publications/2017/Oct/Electricity-storage-and-renewables-costs-and-markets

[25] Larcher, D., & Tarascon, J. M. (2015). Towards greener and more sustainable batteries for electrical energy storage. *Nature Chemistry, 7*(1), 19–29. https://doi.org/10.1038/nchem.2085

[26] Kollimalla, S. K., Mishra, M. K., & Narasamma, N. L. (2014). Design and Analysis of Novel Control Strategy for Battery and Supercapacitor Storage System. IEEE

Transactions on Sustainable Energy, 5(4), 1137–1144. https://doi.org/10.1109/TSTE.2014.2336896.

[27] IRENA. "Electricity Storage and Renewables: Costs and Markets to 2030." International Renewable Energy Agency. 2017.

[28] Larcher, D., & Tarascon, J.M. "Towards greener and more sustainable batteries for electrical energy storage." Nature Chemistry. 2015, 7(1), 19-29.

[29] Barbosa, L. S., Bogdanov, D., Vainikka, P., & Breyer, C. (2017). A Review of the Technical and Economic Implications of Connecting Residential PV Systems to the Grid. Energy Procedia, *115*, 162–173. https://doi.org/10.1016/j.egypro.2017.05.017.

[30] Castaneda, M., Zapata, S., Cherni, J., Dyner, I., & Jurasz, J. (2020). Techno-economic analysis of PV battery systems in Germany: The key role of subsidies. Energy Policy, *139*, 111350. https://doi.org/10.1016/j.enpol.2020.111350

[31] Zakeri, B., & Syri, S. (2015). Electrical energy storage systems: A comparative life cycle cost analysis. Renewable and Sustainable Energy Reviews, *42*, 569–596. https://doi.org/10.1016/j.rser.2014.10.011.

[32] IRENA. (2020). Electricity storage valuation framework: Assessing system value and ensuring project viability. International Renewable Energy Agency

[33] Luo, X., Wang, J., Dooner, M., & Clarke, J. (2015). Overview of current development in electrical energy storage technologies and the application potential in power system operation. Applied Energy, 137, 511–536. https://doi.org/10.1016/j.apenergy.2014.09.081.

[34] Erickson, R. W., & Maksimović, D. (2001). *Fundamentals of Power Electronics* (2nd ed.). Springer US. https://doi.org/10.1007/b100747.

[35] Mohan, N., Undeland, T. M., & Robbins, W. P. (2003). *Power Electronics: Converters, Applications, and Design* (3rd ed.). John Wiley & Sons. ISBN: 978-0-471-22693-2.

[36] Chen, H., Li, J., Wei, S., & Wang, Q. (2021). Real-time energy management for fuel cell electric vehicle using equivalent consumption minimization strategy. IEEE Transactions on Transportation Electrification, *7*(3), 1330-1341.https://doi.org/10.1109/TTE.2020.3044618.

[37] Lasseter, R. H. (2002). Microgrids. In 2002 IEEE Power Engineering Society Winter Meeting. Conference Proceedings (Cat. No. 02CH37309) (Vol. 1, pp. 305-308). IEEE. https://doi.org/10.1109/PESW.2002.985003.

[38] Uzunoglu, M., & Alam, M. S. (2007). Dynamic modeling, design and simulation of a PEM fuel cell/ultra-capacitor hybrid system for vehicular applications. Energy Conversion and Management, *48*(5), 1544-1553.https://doi.org/10.1016/j.enconman.2006.11.019.

[39] IRENA. (2020). Electricity storage valuation framework: Assessing system value and ensuring project viability. International Renewable Energy Agency .

[40] Mongird, K., Fotedar, V., Viswanathan, V., Koritarov, V., Balducci, P., Hadjerioua, B., & Alam, J. (2019). Energy Storage Technology and Cost Characterization Report. U.S. Department of Energy, Pacific Northwest National Laboratory. PNNL-28866. https://doi.org/10.2172/1573487.

[41] IRENA. (2020). Innovation Outlook: Smart Charging for Electric Vehicles. International Renewable Energy Agency, Abu Dhabi, https://www.irena.org/publications/2020/Nov/Innovation-Outlook-Smart-Charging-for-Electric-Vehicles.

[42] Dunn, B., Kamath, H., & Tarascon, J. M. (2011). Electrical energy storage for the grid: a battery of choices. Science, https://doi.org/10.1126/science.1212741.

[43] Lund, H., Østergaard, P. A., Connolly, D., & Mathiesen, B. V. (2017). Smart energy and smart energy systems. Energy, https://doi.org/10.1016/j.energy.2017.05.123

[44] Dragičević, T., Lu, X., Vasquez, J. C., & Guerrero, J. M. (2016). DC microgrids—Part I: A review of control strategies and stabilization techniques. IEEE Transactions on Power Electronics, *31*(7), 4876-4891. https://doi.org/10.1109/TPEL.2015.2478859.

[45] Hammerstrom, D. J. (2007). AC versus DC distribution systems-did we get it right?. In 2007 IEEE Power Engineering Society General Meeting (pp. 1-5). IEEE. https://doi.org/10.1109/PES.2007.385537.

[46] Kakigano, H., Miura, Y., & Ise, T. (2010). Low-Voltage Bipolar-Type DC Microgrid for Super High Quality Distribution. *IEEE Transactions on Power Electronics*, 25(12), 3066–3075. https://doi.org/10.1109/TPEL.2010.2077682.

[47] Ferrara, M., Fabrizio, E., Virgone, J., & Filippi, M. (2014). A simulation-based optimization method for cost-optimal analysis of nearly Zero Energy Buildings. Energy and Buildings, *84*, 442–457. https://doi.org/10.1016/j.enbuild.2014.08.031.

[48] Marnay, C., Chatzivasileiadis, S., & Abbey, C. (2015). Microgrid evolution roadmap. In 2015 International Symposium on Smart Electric Distribution Systems and Technologies (EDST) (pp. 139-144). IEEE. https://doi.org/10.1109/SEDST.2015.7315203.

[49] Hirsch, A., Parag, Y., & Guerrero, J. (2018). Microgrids: A review of technologies, key drivers, and outstanding issues. Renewable and Sustainable Energy Reviews, *90*, 402-411. https://doi.org/10.1016/j.rser.2018.03.040.

[50] Thounthong, P., Rael, S., & Davat, B. (2009). Energy management of fuel cell/battery/supercapacitor hybrid power source for vehicle applications. Journal of Power Sources, *193*(1), 376-385.https://doi.org/10.1016/j.jpowsour.2009.02.073.

[51] Lazard. (2023). Lazard's Levelized Cost of Storage Analysis (Version 9.0). Lazard Ltd. https://www.lazard.com/research-insights/2023-levelized-cost-of-energyplus/.

[52] Hesse, H., Schimpe, M., Kucevic, D., & Jossen, A. (2017). Lithium-ion battery storage for the grid—A review of stationary battery storage system design tailored for applications in modern power grids. Energies, https://doi.org/10.3390/en10122107

[53] Guerrero, J. M., Vasquez, J. C., Matas, J., de Vicuña, L. G., & Castilla, M. (2011). Hierarchical Control of Droop-Controlled AC and DC Microgrids—A General Approach

Toward Standardization. *IEEE Transactions on Industrial Electronics*, 58(1), 158–172. https://doi.org/10.1109/TIE.2010.2066534.

[54] Rocabert, J., Luna, A., Blaabjerg, F., & Rodríguez, P. (2012). Control of Power Converters in AC Microgrids. *IEEE Transactions on Power Electronics*, 27(11), 4734–4749. https://doi.org/10.1109/TPEL.2012.2199334.

[55] Khan, M. N. H., Forouzesh, M., Siwakoti, Y. P., Li, L., Kerekes, T., & Blaabjerg, F. (2020). Transformerless inverter topologies for single-phase photovoltaic systems: A comparative review. IEEE Journal of Emerging and Selected Topics in Power Electronics, 8(1), 805-835. https://doi.org/10.1109/JESTPE.2019.2950351

[56] Bhattacharjee, A. K., Kutkut, N., & Divan, D. M. (2019). Review of modular power conversion solutions for fast charging of electric vehicles. IEEE Transactions on Power Electronics, 34(2), 1352-1368 **:** https://doi.org/10.1109/TPEL.2018.2832198

[57] Tenti, P., Mattavelli, P., & Tedeschi, E. (2011). Grid-connected renewable energy sources: Issues of synchronization and power/energy management. In *2011 IEEE International Symposium on Industrial Electronics* (pp. 941-946). IEEE. https://doi.org/10.1109/ISIE.2011.5984332

[58] Micallef, A., Apap, M., Spiteri-Staines, C., & Guerrero, J. M. (2014). Reactive power sharing and voltage harmonic distortion compensation in droop controlled islanded microgrids. *IEEE Transactions on Smart Grid, 5*(3), 1149-1158. https://doi.org/10.1109/TSG.2013.2294275

[59] Rashid, M. H. (Ed.). (2011). *Power electronics handbook: Devices, circuits and applications* (3rd ed.). Butterworth-Heinemann.

[60] Lopes, J. A. P., Soares, F. J., & Almeida, P. M. R. (2011). Integration of electric vehicles in the electric power system. *Proceedings of the IEEE, 99*(1), 168-183. https://doi.org/10.1109/JPROC.2010.2066250

[61] Bragard, M., Soltau, N., Thomas, S., & Doncker, R. W. D. (2010). The balance of renewable sources and user demands in grids: Power electronics for modular battery energy storage systems. *IEEE Transactions on Power Electronics, 25*(12), 3049-3056. https://doi.org/10.1109/TPEL.2010.2049366

[62] Gungor, V. C., Sahin, D., Kocak, T., Ergut, S., Buccella, C., Cecati, C., & Hancke, G. P. (2011). Smart grid technologies: Communication technologies and standards. *IEEE Transactions on Industrial Informatics, 7*(4), 529-539. https://doi.org/10.1109/TII.2011.2166794

[63] Vinnikov, D., & Roasto, I. (2011). Quasi-Z-source-based isolated DC/DC converters for distributed power generation. *IEEE Transactions on Industrial Electronics, 58*(1), 192-201. https://doi.org/10.1109/TIE.2010.2044116

[64] Wai, R. J., & Duan, R. Y. (2005). High-step-up converter with coupled-inductor. IEEE Transactions on Power Electronics, 20(5), 1025-1035. https://doi.org/10.1109/TPEL.2005.854023

[65] Bouscayrol, A., & Lhomme, W. (2018). Energetic macroscopic representation of a fuel cell-supercapacitor system for vehicle. *IFAC-PapersOnLine, 51*(9), 223-228. https://doi.org/10.1016/j.ifacol.2018.07.038

[66] Garcia, O., Zumel, P., de Castro, A., & Cobos, A. (2006). Automotive DC-DC bidirectional converter made with many interleaved buck stages. *IEEE Transactions on Power Electronics, 21*(3), 578-586. https://doi.org/10.1109/TPEL.2006.872372

[67] Huber, L., & Jovanović, M. M. (2000). A design approach for server power supplies for networking applications. In *Proceedings of IEEE International Telecommunications Energy Conference* (pp. 116-124). IEEE. https://doi.org/10.1109/INTLEC.2000.884256

[68] Kim, J. H., & Lee, J. H. (2009). A high efficiency phase-shifted full-bridge converter with a dual auxiliary resonant circuit for an electric vehicle battery charger. *Journal of Power Electronics, 9*(6), 909-919

[69] Tseng, K. C., Huang, C. C., & Shih, W. Y. (2013). A high step-up converter with a voltage multiplier module for a photovoltaic system. *IEEE Transactions on Power Electronics, 28*(6), 3047-3057. https://doi.org/10.1109/TPEL.2012.2221482

[70] Na, W., & Chen, Q. (2020). A novel MPPT method for enhancing energy conversion efficiency of PEM fuel cell systems under variant air stoichiometry. *International Journal of Hydrogen Energy, 45*(15), 9118-9130. https://doi.org/10.1016/j.ijhydene.2020.01.148

[71] Zhang, N., Sutanto, D., & Muttaqi, K. M. (2015). A review of topologies of three-port DC–DC converters for the integration of renewable energy and energy storage system. *Renewable and Sustainable Energy Reviews, 56*, 388-401. https://doi.org/10.1016/j.rser.2015.11.066

[72] Maksimović, D., & Zane, R. (2007). Small-signal discrete-time modeling of digitally controlled PWM converters. *IEEE Transactions on Power Electronics, 22*(6), 2552-2556. https://doi.org/10.1109/TPEL.2007.909248

[73] Noussan, M., Litzenburger, L., & Jarre, M. (2020). Review of operation control strategies for hybrid PV-battery systems. *Renewable and Sustainable Energy Reviews, 133*, 110239. https://doi.org/10.1016/j.rser.2020.110239

[74] Rodriguez, J., & Ammann, U. (2008). *Predictive control of power converters and electrical drives*. John Wiley & Sons. https://doi.org/10.1002/9780470774513

[75] Kwon, J. M., Kwon, B. H., & Nam, K. H. (2008). Three-phase photovoltaic system with three-level boosting MPPT control. *IEEE Transactions on Power Electronics, 23*(5), 2319-2327. https://doi.org/10.1109/TPEL.2008.2001906

[76] Kwasinski, A. (2011). Identification of feasible topologies for multiple-input DC-DC converters. *IEEE Transactions on Power Electronics, 26*(9), 2374-2387. https://doi.org/10.1109/TPEL.2011.2107895

[77] Ing, W., Lai, C. H., Wong, S. H. W., & Wong, M. L. D. (2018). A comprehensive study of battery-supercapacitor hybrid energy storage system for standalone PV power system in rural electrification. *Applied Energy, 224*, 340-356. https://doi.org/10.1016/j.apenergy.2018.04.106

[78] Kim, J., Guerrero, J. M., Rodriguez, P., Teodorescu, R., & Nam, K. (2011). Mode adaptive droop control with virtual output impedances for an inverter-based flexible AC microgrid. *IEEE Transactions on Power Electronics, 26*(3), 689-701. https://doi.org/10.1109/TPEL.2010.2091685

[79] MChaudhary, S. K., Guerrero, J. M., & Teodorescu, R. (2014). Enhancing the capacity of the AC microgrid using isolated bidirectional DC–DC converter controlled by

decentralized control scheme. *IEEE Transactions on Power Electronics, 29*(9), 4580-4589. https://doi.org/10.1109/TPEL.2013.2292036

[80] Bose, B. K. (2006). *Power electronics and motor drives: Advances and trends*. Academic Press.

[81] Bidram, A., & Davoudi, A. (2012). Hierarchical structure of microgrids control system. *IEEE Transactions on Smart Grid, 3*(4), 1963-1976. https://doi.org/10.1109/TSG.2012.2197425

[82] Sannino, A., Postiglione, G., & Bollen, M. H. (2003). Feasibility of a DC network for commercial facilities. *IEEE Transactions on Industry Applications, 39*(5), 1499-1507. https://doi.org/10.1109/TIA.2003.816535

[83] Guerrero, J. M., Loh, P. C., Lee, T. L., & Chandorkar, M. (2013). Advanced control architectures for intelligent microgrids—Part II: Power quality, energy storage, and AC/DC microgrids. *IEEE Transactions on Industrial Electronics, 60*(4), 1263-1270. https://doi.org/10.1109/TIE.2012.2196889

[84] Peyghami, S., Mokhtari, H., & Blaabjerg, F. (2018). A review on microgrid ac/dc voltage and power quality issues. *IEEE Electrification Magazine, 6*(2), 48-55. https://doi.org/10.1109/MELE.2018.2815660

[85] Kim, Y. H., Kim, J. H., & Moon, G. W. (2013). A new standby structure using a bidirectional converter for renewable energy systems. *IEEE Transactions on Industrial Electronics, 60*(11), 5090-5098. https://doi.org/10.1109/TIE.2012.2224077

[86] Wen, B., Boroyevich, D., Burgos, R., Mattavelli, P., & Shen, Z. (2016). Analysis of D-Q small-signal impedance of grid-tied inverters. *IEEE Transactions on Power Electronics, 31*(1), 675-687. https://doi.org/10.1109/TPEL.2015.2398192

[87] Middlebrook, R. D., & Cuk, S. (1977). A general unified approach to modelling switching-converter power stages. *International Journal of Electronics, 42*(6), 521-550. https://doi.org/10.1080/00207217708900678

[88] Sanders, S. R., Noworolski, J. M., Liu, X. Z., & Verghese, G. C. (1991). Generalized averaging method for power conversion circuits. *IEEE Transactions on Power Electronics, 6*(2), 251-259. https://doi.org/10.1109/63.76811

[89] Holmgren, W. F., Hansen, C. W., & Mikofski, M. A. (2018). pvlib python: A python package for modeling solar energy systems. *Journal of Open Source Software, 3*(29), 884. https://doi.org/10.21105/joss.00884

[90] Prodic, A., Maksimović, D., & Erickson, R. W. (2003). Design and implementation of a digital PWM controller for a high-frequency switching DC-DC power converter. *IEEE Transactions on Power Electronics, 18*(1), 93-103. https://doi.org/10.1109/TPEL.2002.807131

[91] Hemi, H., Ghouili, J., & Cheriti, A. (2015). A real time fuzzy logic power management strategy for a fuel cell vehicle. *Energy Conversion and Management, 91*, 397-405. https://doi.org/10.1016/j.enconman.2014.12.037

[92] Baneshi, M., & Hadianfard, F. (2016). Techno-economic feasibility of hybrid diesel/PV/wind/battery electricity generation systems for non-residential large electricity consumers under southern Iran climate conditions. *Energy Conversion and Management, 127*, 233-244. https://doi.org/10.1016/j.enconman.2016.09.008

[93] Chen, X., Zhang, H., Xu, Z., Nielsen, C. P., McElroy, M. B., Lv, J., & Chen, Y. (2018). Examination of fleet types and charging modes for electric vehicles on emissions under various penetrations of wind power. *Nature Energy, 3*, 413-421. https://doi.org/10.1038/s41560-018-0133-0

[94] Wen, B., Boroyevich, D., Burgos, R., Mattavelli, P., & Shen, Z. (2016). Analysis of D-Q Small-Signal Impedance of Grid-Tied Inverters. *IEEE Transactions on Power Electronics*, 31(1), 675–687.https://doi.org/10.1109/TPEL.2015.2398192.

[95] Zhao, J., & Lam, K. P. (2018). A review of occupant behavior models for building performance simulation. *Building Simulation, 11*(5), 899-914. https://doi.org/10.1007/s12273-018-0444-x

[96] Tuhus-Dubrow, D., & Krarti, M. (2010). Genetic-algorithm based approach to optimize building envelope design for residential buildings. *Building and Environment, 45*(7), 1574-1581. https://doi.org/10.1016/j.buildenv.2010.01.005

[97] Holmgren, W. F., Hansen, C. W., & Mikofski, M. A. (2018). *pvlib python: a python package for modeling solar energy systems*. Journal of Open Source Software, 3(29), 884. https://doi.org/10.21105/joss.00884

[98] Emadi, A., & Ehsani, M. (2000). Multi-converter power electronic systems: Definition and applications. In *2000 IEEE 31st Annual Power Electronics Specialists Conference* (Vol. 1, pp. 123-129). IEEE. https://doi.org/10.1109/PESC.2000.878776

[99] Kwasinski, A., & Krein, P. T. (2007). A microgrid-based telecom power system using modular multiple-input power converters. In *INTELEC 07-29th International Telecommunications Energy Conference* (pp. 807-814). IEEE. https://doi.org/10.1109/INTLEC.2007.4448915

[100] Tseng, K. C., & Huang, C. C. (2014). High step-up high-efficiency interleaved converter with voltage multiplier module for renewable energy system. *IEEE Transactions on Industrial Electronics, 61*(3), 1311-1319. https://doi.org/10.1109/TIE.2013.2257150

[101] Bevrani, H., Ghosh, A., & Ledwich, G. (2010). Renewable energy sources and frequency regulation: Survey and new perspectives. *IET Renewable Power Generation, 4*(5), 438-457. https://doi.org/10.1049/iet-rpg.2009.0049

[102] Erickson, R. W. (2004). Some topologies of high-frequency transformers in DC-DC converters. In *2004 IEEE 35th Annual Power Electronics Specialists Conference (PESC)* (Vol. 1, pp. 48-53). IEEE. https://doi.org/10.1109/PESC.2004.1354681

[103] Belkaid, A., Colak, I., & Kayisli, K. (2017). A comprehensive study of different photovoltaic peak power tracking methods. In *2017 6th IEEE International Conference on Renewable Energy Research and Applications (ICRERA)* (pp. 1073-1079). IEEE. https://doi.org/10.1109/ICRERA.2017.8191217

[104] L., Hadji, S., Belkaid, A., Colak, I., & Bayindir, R. (2022). Design of a buck converter battery charging controller in PV plant. In *2022 10th International Conference on Smart*

Grid (icSmartGrid) (pp. 214-220). IEEE. https://doi.org/10.1109/icSmartGrid55722.2022.9848640

[105] Ndiaye, A., Thiaw, L., & Sow, G. (2015). Application of new modeling and control for grid connected photovoltaic systems based on artificial intelligence. *Journal of Electrical and Electronic Engineering Research*, 7(1), 1-10.

[106] Eltamaly, A. M., Al-Saud, M. S., & Abokhalil, A. G. (2020). A novel scanning bat algorithm strategy for maximum power point tracker of partially shaded photovoltaic energy systems. *Ain Shams Engineering Journal*, 11(4), 1093-1103. https://doi.org/10.1016/j.asej.2020.02.010

[107] Mostefa, K., & El Madjid, B. (2017). Artificial intelligence-based maximum power point tracking controllers for photovoltaic systems: Comparative study. *Renewable and Sustainable Energy Reviews*, 69, 369-386. https://doi.org/10.1016/j.rser.2016.11.125

[108] Chandra, S., & Gaur, P. (2020). Radial basis function neural network technique for efficient maximum power point tracking in solar photovoltaic system. *Procedia Computer Science*, 167, 2354-2363. https://doi.org/10.1016/j.procs.2020.03.288

[109] Robles-Algarin, C., Restrepo-Leal, D., & Castro, A. O. (2019). Data from multimodal functions based on an array of photovoltaic modules and an approximation with artificial neural networks as a scenario for testing optimization algorithms. *Data in Brief*, 27, 104669. https://doi.org/10.1016/j.dib.2019.104669

[110] Kopal, I., Harnicarova, M., Valicek, J., Krmela, J., & Lukac, O. (2019). Radial basis function neural network-based modeling of the dynamic thermomechanical response and damping behavior of thermoplastic elastomer systems. *Polymers*, 11(6), 1041. https://doi.org/10.3390/polym11061041

[111] Moayedi, H., Aghel, B., Vaferi, B., Kok Foong, L., & Bui, D. T. (2020). The feasibility of Levenberg-Marquardt algorithm combined with imperialist competitive computational method predicting drag reduction in crude oil pipelines. *Journal of Petroleum Science and Engineering*, 185, 106634. https://doi.org/10.1016/j.petrol.2019.106634

[112] Chtita, S., Motahhir, S., & El Ghzizal, A. (2024). A new design and embedded implementation of a low-cost maximum power point tracking charge controller for stand-

alone photovoltaic systems. *Energy Technology*, 12(1), 2301324. https://doi.org/10.1002/ente.202301324

[113] Ba, A., Ndiaye, A., Ndiaye, E. M., & Mbodji, S. (2023). Power optimization of a photovoltaic system with artificial intelligence algorithms over two seasons in tropical area. *MethodsX*, 10, 101959. https://doi.org/10.1016/j.mex.2022.101959

[114] Belkaid, A., Kayisli, K., Colak, I., Hadji, S., & Guenounou, O. (2024). Smart power conditioning unit utilizing enhanced Inc-Con MPPT for photovoltaic power plants. *International Journal of Smart Grid*, 8(1), 41-45. https://doi.org/10.20508/ijsmartgrid.v8i1.330.g335

[115] Neath, M. J., Swain, A. K., Madawala, U. K., & Thrimawithana, D. J. (2014). An optimal PID controller for a bidirectional inductive power transfer system using multiobjective genetic algorithm. *IEEE Transactions on Power Electronics*, 29(3), 1523-1531. https://doi.org/10.1109/TPEL.2013.2262710`

[116] Aoughlis, C., Belkaid, A., Kacimi, M. A., Colak, I., Guenounou, O., Bakir, T., & Brikh, L. (2024). A novel dynamic and self-adaptive InCre technique based on PI control and EO optimization for hybrid PV-TEG conversion systems. *Electric Power Components and Systems*, 52(9), 1569-1580. https://doi.org/10.1080/15325008.2023.2296964

[117] Kouro, S., & Cortés, P. (2018). Model predictive control for renewable energy and storage systems in microgrids. *IEEE Transactions on Industrial Electronics*, 65(8), 6514-6528. https://doi.org/10.1109/TIE.2017.2784342

[118] Vivas, F. J., & de las Heras, A. (2020). Predictive control strategies for standalone photovoltaic systems with battery storage. *Renewable Energy*, 147, 1674-1686. https://doi.org/10.1016/j.renene.2019.09.098

[119] A.Belkaid, I.Colak, K.Kayisli, « A Comprehensive Study of different Photovoltaic Peak Power Tracking Methods », pp: 1073-1079, 6th IEEE International Conference on Renewable Energy Research and Applications, ICRERA 2017, 5 - 8 November 2017, San Diego, California, USA.

[120] Bayindir, R., Colak, I., & Belkaid, A. (2021). Smart grid technologies: Comprehensive review of challenges and opportunities. *International Journal of Energy Research, 45*(12), 17519-17542. https://doi.org/10.1002/er.6974

[121] Sow, G., Ndiaye, A., & Thiaw, L. (2016). Artificial intelligence techniques for photovoltaic systems: A comprehensive review. *Renewable and Sustainable Energy Reviews, 63*, 334-349. https://doi.org/10.1016/j.rser.2016.05.071

[122] Abokhalil, A. G., Al-Saud, M. S., & Eltamaly, A. M. (2021). A novel hybrid maximum power point tracking technique for partially shaded photovoltaic systems. *Energy Conversion and Management, 228*, 113697. https://doi.org/10.1016/j.enconman.2020.113697

[123] Valicek, J., Harnicarova, M., & Kopal, I. (2020). Advanced materials for energy storage applications: A neural network approach to property prediction. *Materials Today Communications, 25*, 101521. https://doi.org/10.1016/j.mtcomm.2020.101521

[124] Aghel, B., Moayedi, H., & Vaferi, B. (2021). Machine learning applications in energy systems: A comprehensive review. *Energy Reports, 7*, 7854-7872. https://doi.org/10.1016/j.egyr.2021.10.053

[125] Mbodji, S., Ba, A., & Ndiaye, E. M. (2022). Performance analysis of AI-based MPPT controllers in tropical climates: A two-year case study. *Energy for Sustainable Development, 70*, 386-399. https://doi.org/10.1016/j.esd.2022.08.014

[126] Guenounou, O., Belkaid, A., & Colak, I. (2023). Enhanced incremental conductance MPPT algorithm with adaptive step size for fast-changing irradiance conditions. *Solar Energy, 262*, 111845. https://doi.org/10.1016/j.solener.2023.111845

[127] Thrimawithana, D. J., Madawala, U. K., & Neath, M. J. (2016). A generalized steady-state model for bidirectional inductive power transfer systems. *IEEE Transactions on Power Electronics, 31*(5), 3473-3484. https://doi.org/10.1109/TPEL.2015.2462121

[128] Kacimi, M. A., Aoughlis, C., & Belkaid, A. (2022). Dynamic modeling and control of hybrid renewable energy systems: A comparative study. *Energy Conversion and Management, 252*, 115098. https://doi.org/10.1016/j.enconman.2021.115098

[129] Mattavelli, P., Tenti, P., & Tedeschi, E. (2012). Grid-connected renewable energy systems: Control and power quality issues. *IEEE Transactions on Power Electronics, 27*(6), 2753-2767. https://doi.org/10.1109/TPEL.2011.2177874

[130] de las Heras, A., & Vivas, F. J. (2021). Optimal sizing and control of standalone photovoltaic systems with hybrid storage: A comparative analysis. *Journal of Energy Storage, 44*, 103362. https://doi.org/10.1016/j.est.2021.103362

[131] Cortés, P., & Kouro, S. (2019). Model predictive control of power converters: Basic concepts and applications in microgrids. *IEEE Industrial Electronics Magazine, 13*(2), 36-49. https://doi.org/10.1109/MIE.2019.2904471

[132] Brikh, L., Bakir, T., & Aoughlis, C. (2023). Thermoelectric generators integration in photovoltaic systems: Efficiency enhancement and cost analysis. *Applied Thermal Engineering, 234*, 121217. https://doi.org/10.1016/j.applthermaleng.2023.121217

[133] Hadji, S., Larbi, L., & Belkaid, A. (2021). Design and implementation of an efficient battery charging controller for large-scale PV plants. *Journal of Energy Storage, 44*, 103291. https://doi.org/10.1016/j.est.2021.103291

[134] Kayisli, K., Colak, I., & Belkaid, A. (2018). A comprehensive review of maximum power point tracking algorithms for photovoltaic systems. *International Journal of Renewable Energy Research, 8*(2), 885-906.

[135] Colak, I., Bayindir, R., & Belkaid, A. (2020). Smart grid infrastructure and applications: Current status and future directions. *IEEE Access, 8*, 180512-180534. https://doi.org/10.1109/ACCESS.2020.3028194

[136] Belkaid, A., Colak, I., & Kayisli, K. (2019). Performance comparison of different MPPT techniques for photovoltaic systems under partial shading conditions. *International Journal of Photoenergy, 2019*, 1-15. https://doi.org/10.1155/2019/5268472

.

Appendices

Appendix A

A. Open-loop simulation of the system (chapter 3)

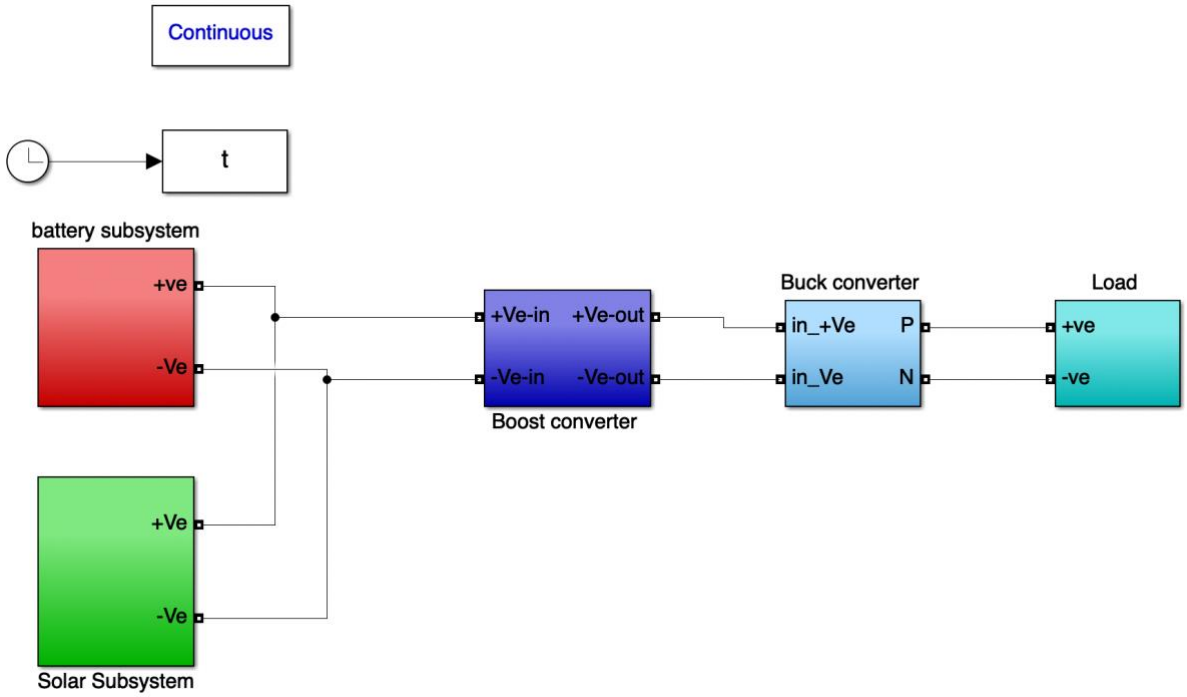

Appendix B

B. 1. Photovoltaic subsystem:

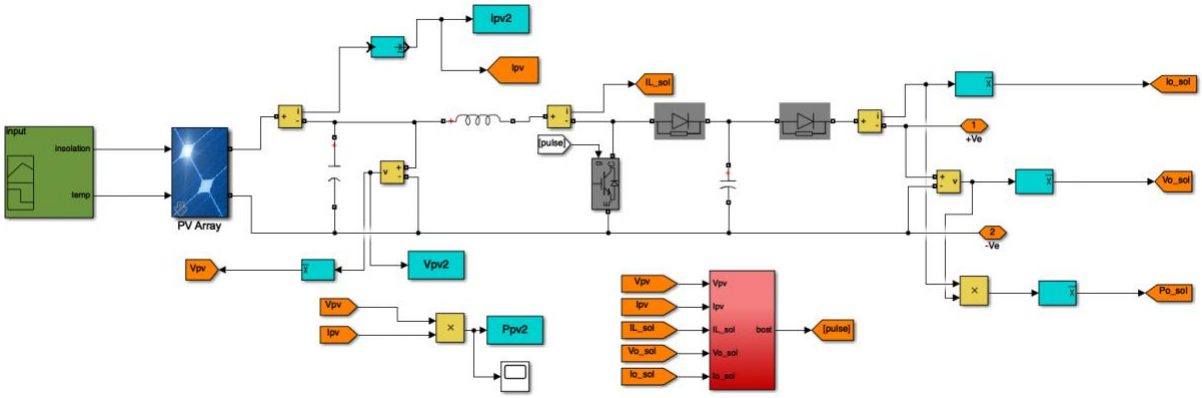

B.2. Battery subsystem:

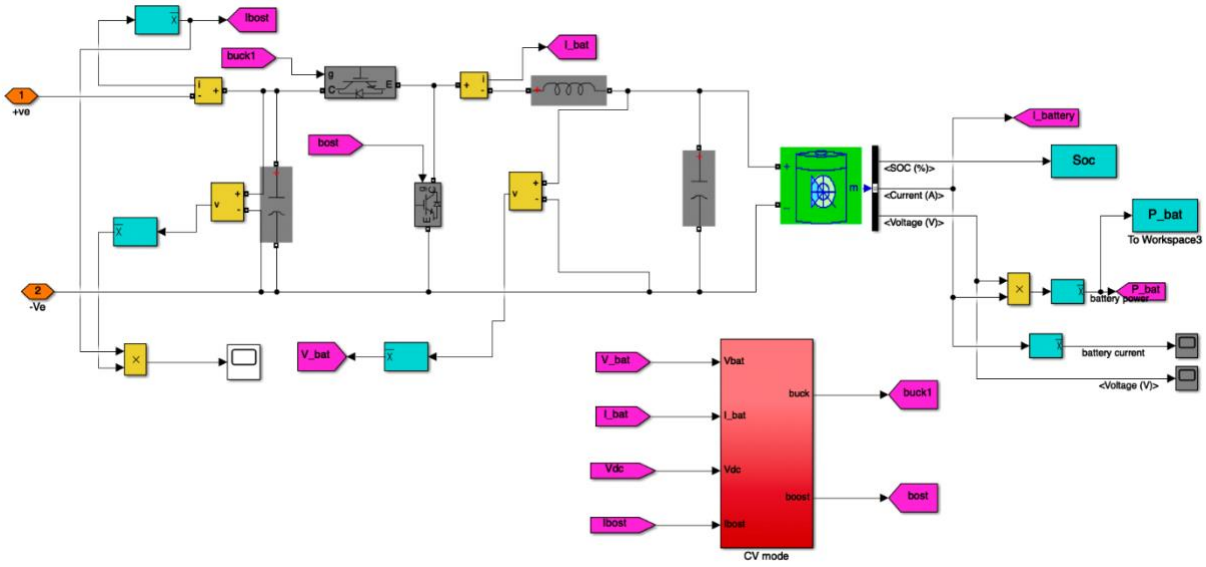

Appendix C

- **C.1. LOAD of system in MATLAB/ Simulink:**

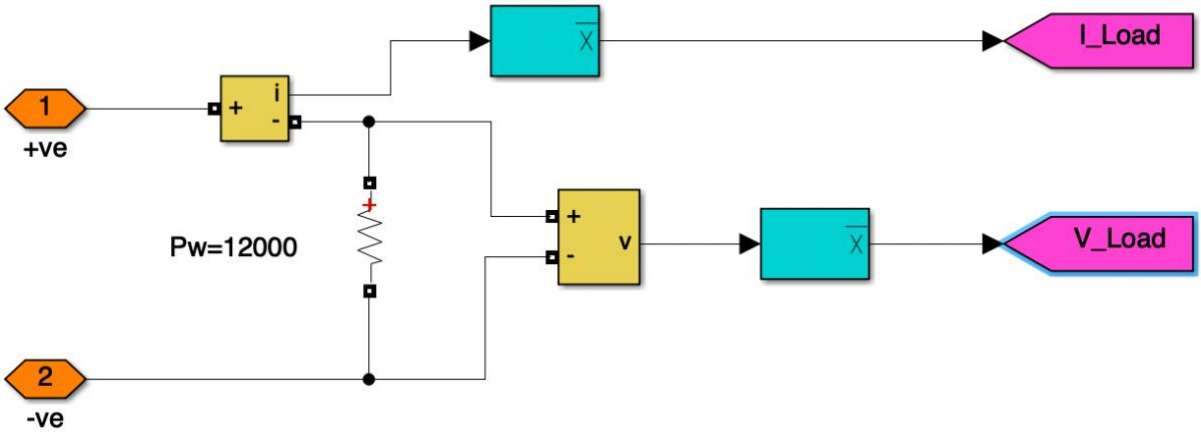

- **P&O Algorithm:**

Step 1: Start

Step 2: Read variables $V(n)$ and $I(n)$.

Step 3: Calculate power: $P(n) = V(n) \times I\ (n)$

Step 4: Call previous values of $P$and$V$ from the memory.

$P(n-1)$ and$V(n-1)$

Step 5: Calculate the change in power dP and change in voltage dV using:

$$dV = V(n) - V(n-1) \quad \text{and} \quad dP = P(n) - P(n-1)$$

Step 6: If $dP = 0$, Then no change in duty ratio is required and GOTO Step 7.

Else If $(dP.dV) > 0$, Then increase the duty ratio by ΔD and GOTO Step 7.

Else decrease the duty ratio by ΔD and GOTO Step 7

Step7: return.

- **P&O in MATLAB /Simulink:**

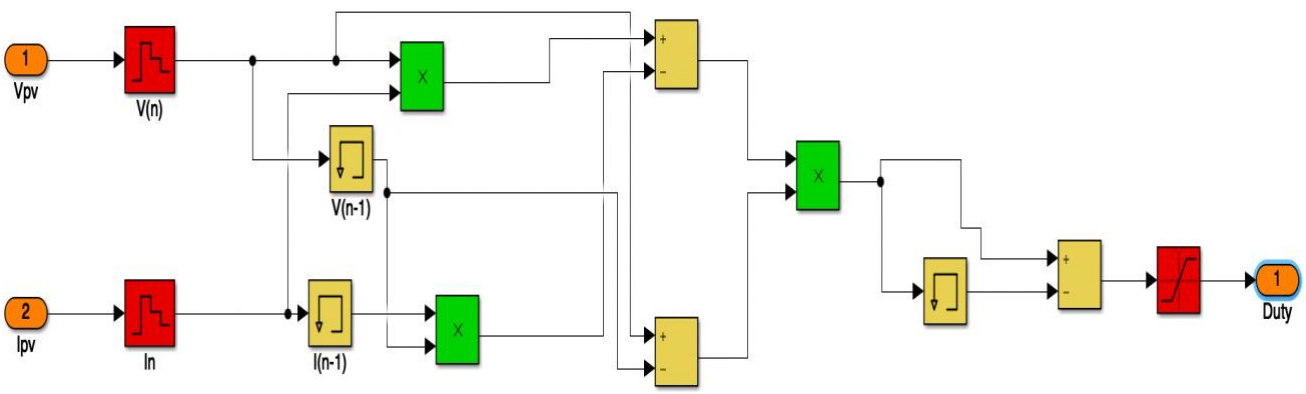

Design of a battery charger circuit with intelligent control of maximum photovoltaic power point tracking

Abstract

Solar photovoltaic energy plays a vital role in addressing global energy challenges due to its adaptability, scalability, and ability to meet diverse industrial and consumer demands. Compared to other renewable sources, PV systems offer long-term electricity generation without mechanical components, making them a reliable and low-maintenance option. However, their power output is inherently variable, with nonlinear voltage characteristics, leading to challenges related to intermittency. To ensure efficient energy utilization, maximum power point tracking (MPPT) is essential for optimizing power conversion at any given moment. This study focuses on the simulation of a battery charging circuit incorporating MPPT to maximize power extraction from PV modules under varying solar irradiance and temperature conditions in an off-grid system. Various MPPT techniques have been developed, ranging from conventional to advanced approaches, depending on environmental factors and system requirements. This work specifically compares two widely used methods: Perturb and Observe (P&O) and Artificial Neural Networks (ANN). Chapters 1 through 3 elaborate on the system architecture of PV-battery configurations, component modeling, power converter design, and control strategies. The results demonstrate that the ANN-based approach provides faster and more stable maximum power point tracking, with reduced oscillations and superior adaptability to weather variations compared to the P&O method.

Keywords: Artificial neural networks - battery - maximum power point tracking - perturbation and observation -photovoltaic.

Conception d'un circuit de charge de batterie avec commande intelligente de la recherche du point de puissance maximale photovoltaïque.

Résumé

L'énergie solaire photovoltaïque joue un rôle essentiel dans la réponse aux défis énergétiques mondiaux grâce à sa flexibilité, sa modularité et sa capacité à répondre à des besoins variés, tant industriels que domestiques. Comparée à d'autres sources renouvelables, la technologie photovoltaïque permet une production électrique durable sans pièces mobiles, ce qui en fait une solution fiable et peu exigeante en maintenance. Cependant, la production d'énergie est

intermittente et présente des caractéristiques tension-courant non linéaires, ce qui rend nécessaire l'optimisation du point de puissance maximale (MPPT) pour maximiser le rendement énergétique. Cette étude se concentre sur la modélisation et la simulation d'un système de charge de batterie intégrant un algorithme MPPT, afin d'extraire le maximum de puissance des modules PV sous des conditions variables d'ensoleillement et de température dans un système hors réseau. Différentes techniques MPPT ont été développées, allant des méthodes conventionnelles aux approches intelligentes, en fonction des conditions environnementales et des exigences du système. Ce travail compare plus particulièrement deux stratégies largement utilisées : la méthode Perturbation et Observation (P&O) et celle basée sur les réseaux de neurones artificiels (ANN). Les chapitres 1 à 3 détaillent respectivement l'architecture des systèmes PV-batterie, la modélisation des composants, la conception des convertisseurs et les stratégies de contrôle. Les résultats montrent que l'approche ANN offre un suivi plus rapide et plus stable du point de puissance maximale, avec moins d'oscillations et une meilleure adaptation aux variations météorologiques que la méthode P&O.

Mots-clés : Réseaux de neurones artificiels - batterie - suivi du point de puissance maximale - perturbation et observation - photovoltaïque

تصميم دائرة شحن بطارية ذات تحكم ذكي في تتبع نقطة القدرة القصوى للطاقة الشمسية

الملخص.

تلعب الطاقة الشمسية الكهروضوئية دورًا حيويًا في مواجهة التحديات العالمية للطاقة نظرًا لمرونتها وقابليتها للتوسع وقدرتها على تلبية احتياجات صناعية واستهلاكية متنوعة. مقارنة بمصادر الطاقة المتجددة الأخرى، تقدم الأنظمة الكهروضوئية توليدًا كهربائيًا طويل الأمد بدون مكونات ميكانيكية، مما يجعلها خيارًا موثوقًا وقليل الصيانة. ومع ذلك، فإن إنتاج الطاقة متغير بطبيعته، ويتميز بخصائص غير خطية للجهد والتيار، مما يؤدي إلى تحديات تتعلق بالتقطع. لضمان الاستخدام الفعال للطاقة، يعد تتبع نقطة الطاقة القصوى (MPPT) ضروريًا لتحسين تحويل الطاقة في أي لحظة.

تركز هذه الدراسة على محاكاة دائرة شحن البطارية المدمجة مع خوارزمية MPPT لتعظيم استخراج الطاقة من الوحدات الكهروضوئية تحت ظروف إشعاع شمسي ودرجة حرارة متغيرة في نظام معزول. تم تطوير تقنيات MPPT متنوعة، تتراوح بين الأساليب التقليدية والمتقدمة، اعتمادًا على العوامل البيئية ومتطلبات النظام. يقارن هذا العمل على وجه التحديد طريقتين مستخدمتين على نطاق واسع Perturbe and Observe (P&O) :والشبكات العصبية الاصطناعية (ANN).

تفصّل الفصول من 1 إلى 3 هندسة النظام لتكوينات-PV البطارية، ونمذجة المكونات، وتصميم محولات الطاقة، واستراتيجيات التحكم. تظهر النتائج أن نهج ANN يوفر تتبعًا أسرع وأكثر استقرارًا لنقطة الطاقة القصوى، مع تقليل التذبذبات وتكيف أفضل مع التغيرات الجوية مقارنة بطريقة.P&O

الكلمات المفتاحية: الشبكات العصبية الاصطناعية - البطارية - تتبع نقطة القدرة القصوى - طريقة الاضطراب والملاحظة - الخلايا الشمسية (الطاقة الضوئية) .

Abstract

Solar photovoltaic energy plays a vital role in addressing global energy challenges due to its adaptability, scalability, and ability to meet diverse industrial and consumer demands. Compared to other renewable sources, PV systems offer long-term electricity generation without mechanical components, making them a reliable and low-maintenance option. However, their power output is inherently variable, with nonlinear voltage characteristics, leading to challenges related to intermittency. To ensure efficient energy utilization, maximum power point tracking (MPPT) is essential for optimizing power conversion at any given moment. This study focuses on the simulation of a battery charging circuit incorporating MPPT to maximize power extraction from PV modules under varying solar irradiance and temperature conditions in an off-grid system. Various MPPT techniques have been developed, ranging from conventional to advanced approaches, depending on environmental factors and system requirements. This work specifically compares two widely used methods: Perturb and Observe (P&O) and Artificial Neural Networks (ANN). Chapters 1 through 3 elaborate on the system architecture of PV-battery configurations, component modeling, power converter design, and control strategies. The results demonstrate that the ANN-based approach provides faster and more stable maximum power point tracking, with reduced oscillations and superior adaptability to weather variations compared to the P&O method.

Keywords: Artificial neural networks - battery - maximum power point tracking -perturbation and observation - photovoltaic.

Résumé

L'énergie solaire photovoltaïque joue un rôle essentiel dans la réponse aux défis énergétiques mondiaux grâce à sa flexibilité, sa modularité et sa capacité à répondre à des besoins variés, tant industriels que domestiques. Comparée à d'autres sources renouvelables, la technologie photovoltaïque permet une production électrique durable sans pièces mobiles, ce qui en fait une solution fiable et peu exigeante en maintenance. Cependant, la production d'énergie est intermittente et présente des caractéristiques tension-courant non linéaires, ce qui rend nécessaire l'optimisation du point de puissance maximale (MPPT) pour maximiser le rendement énergétique. Cette étude se concentre sur la modélisation et la simulation d'un système de charge de batterie intégrant un algorithme MPPT, afin d'extraire le maximum de puissance des modules PV sous des conditions variables d'ensoleillement et de température dans un système hors réseau. Différentes techniques MPPT ont été développées, allant des méthodes conventionnelles aux approches intelligentes, en fonction des conditions environnementales et des exigences du système. Ce travail compare plus particulièrement deux stratégies largement utilisées : la méthode Perturbation et Observation (P&O) et celle basée sur les réseaux de neurones artificiels (ANN). Les chapitres 1 à 3 détaillent respectivement l'architecture des systèmes PV-batterie, la modélisation des composants, la conception des convertisseurs et les stratégies de contrôle. Les résultats montrent que l'approche ANN offre un suivi plus rapide et plus stable du point de puissance maximale, avec moins d'oscillations et une meilleure adaptation aux variations météorologiques que la méthode P&O.

Mots-clés : Réseaux de neurones artificiels - batterie - suivi du point de puissance maximale - perturbation et observation - photovoltaïque

تصميم دائرة شحن بطارية ذات تحكم ذكي في تتبع نقطة القدرة القصوى للطاقة الشمسية

الملخص.

تلعب الطاقة الشمسية الكهروضوئية دورًا حيويًا في مواجهة التحديات العالمية للطاقة نظرًا لمرونتها وقابليتها للتوسع وقدرتها على تلبية احتياجات صناعية واستهلاكية متنوعة. مقارنة بمصادر الطاقة المتجددة الأخرى، تقدم الأنظمة الكهروضوئية توليدًا كهربائيًا طويل الأمد بدون مكونات ميكانيكية، مما يجعلها خيارًا موثوقًا وقليل الصيانة. ومع ذلك، فإن إنتاج الطاقة متغير بطبيعته، ويتميز بخصائص غير خطية للجهد والتيار، مما يؤدي إلى تحديات تتعلق بالتقطع. لضمان الاستخدام الفعال للطاقة، يعد تتبع نقطة الطاقة القصوى (MPPT) ضروريًا لتحسين تحويل الطاقة في أي لحظة.

تركز هذه الدراسة على محاكاة دائرة شحن البطارية المدمجة مع خوارزمية MPPT لتعظيم استخراج الطاقة من الوحدات الكهروضوئية تحت ظروف إشعاع شمسي ودرجة حرارة متغيرة في نظام معزول. تم تطوير تقنيات MPPT متنوعة، تتراوح بين الأساليب التقليدية والمتقدمة، اعتمادًا على العوامل البيئية ومتطلبات النظام. يقارن هذا العمل على وجه التحديد طريقتين مستخدمتين على نطاق واسع : Perturbe and Observe (P&O)والشبكات العصبية الاصطناعية.(ANN)

تفصّل الفصول من 1 إلى 3 هندسة النظام لتكوينات-PV البطارية، ونمذجة المكونات، وتصميم محولات الطاقة، واستراتيجيات التحكم. تظهر النتائج أن نهج ANN يوفر تتبعًا أسرع وأكثر استقرارًا لنقطة الطاقة القصوى، مع تقليل التذبذبات وتكيف أفضل مع التغيرات الجوية مقارنة بطريقة.P&O

الكلمات المفتاحية: الشبكات العصبية الاصطناعية - البطارية - تتبع نقطة القدرة القصوى - طريقة الاضطراب والملاحظة - الخلايا الشمسية (الطاقة الضوئية) .